Remote video eavesdropping using a software-defined radio platform

Martin Marinov
St Edmund's College

UNIVERSITY OF CAMBRIDGE

A dissertation submitted to the University of Cambridge in partial fulfilment of the requirements for the degree of Master of Philosophy in Advanced Computer Science

University of Cambridge
Computer Laboratory
William Gates Building
15 JJ Thomson Avenue
Cambridge CB3 0FD
United Kingdom

Email: mtm46@cam.ac.uk

June 11, 2014

Declaration

I Martin Marinov of St Edmund's College, being a candidate for the M.Phil in Advanced Computer Science, hereby declare that this report and the work described in it are my own work, unaided except as may be specified below, and that the report does not contain material that has already been used to any substantial extent for a comparable purpose.

Total word count:

`14,744`

Signed:

Date:

Abstract

This dissertation presents a software toolkit for remotely eavesdropping video monitors using a Software Defined Radio (SDR) receiver. It exploits compromising emanations from cables carrying video signals.

Raster video is usually transmitted one line of pixels at a time, encoded as a varying current. This generates an electromagnetic wave that can be picked up by an SDR receiver. The software maps the received field strength of a pixel to a gray-scale shade in real-time. This forms a false colour estimate of the original video signal.

The toolkit uses unmodified off-the-shelf hardware which lowers the costs and increases mobility compared to existing solutions. It allows for additional post-processing which improves the signal-to-noise ratio. The attacker does not need to have prior knowledge about the target video display. All parameters such as resolution and refresh rate are estimated with the aid of the software.

The software consists of a library written in C, a collection of plug-ins for various Software Define Radio (SDR) front-ends and a Java based Graphical User Interface (GUI). It is a multi-platform application, with all native libraries pre-compiled and packed into a single Java jar file.

Acknowledgements

I would like to thank my supervisor, Dr Markus Kuhn, for providing me with the inspiration for the project. He also lent me his USRP 2 software-defined radio device to start my research with before I acquired my own USRP B200. His help with shaping my understanding of the emanated signals and their nature allowed me to come up with the algorithms and implementations that are described in this project. He also tested the early iterations of the system giving me feedback about its performance and user friendliness. He was also able to come up with an analogue preconditioning procedure to improve the signal-to-noise ratio of the USRP B200 hardware.

Contents

Chapter 1

Introduction

Interference is usually regarded as a simple annoyance. It is not difficult to experience TV signal or radio station getting distorted because of a device operating in the vicinity. Manufacturers have to meet certain requirements[1] so that their products do not cause interference with other systems. The truth is that the emanation is linked to the way the emitting device works internally. The interference is generated by alternating currents due to switches, oscillators and other electronic and mechanical components operating inside the device. Therefore it carries some information about the internal state of the device.

This means that a simple annoyance could potentially turn into a security leak, broadcasting sensitive data into the wild. A clever attacker could distinguish different modes of operation or even, as shown in this report, recover raw data that is being processed. The industry standards that manufacturers follow to minimise interference say nothing about the data it may carry. A very sensitive detector can pick up such signals at levels several magnitudes lower than what standards specify as radiation limits.

In the case of video displays the issue is particularly important. Having a secure, encrypted computer system that unintentionally broadcasts its dis-

[1] For the EU this would be EN 55022 [1].

play in clear text does not sound secure at all. The attacker could be fully passive and the breach could never be detected. The repeating nature of the signal, combined with the long video wires that act as antennas, mean that such signals can travel very long distances, allowing practical attacks from vans across the street [2].

However little research has been published into the open literature on the topic. The main reason is possibly the expensive specialised equipment required to conduct experiments with compromising emanations. One of the goals of this project is to address this issue and demonstrate that a practical attack could be undertaken using an affordable software-defined radio receiver.

1.1 History

A compass needle points north when put next to a wire that has current flowing in it. Turning off the current makes the needle twitch i.e. temporary deflecting from the north direction. The same effect could be seen if the current is turned back on. This phenomenon was noticed by the Danish physicist Hans Christian Ørsted in April 1820 [3]. It shows that a changing electric current creates a magnetic field and vice versa. Later this phenomenon was utilised to create the electrical telegraph and allow for long distance communications.

However, the undesired effects of this phenomenon received almost no attention for a couple of decades. British army noticed crosstalk between telephone wires during the Nile and Suakin expedition in 1884-85 [4]. The first reported exploitation of the phenomenon was in 1914 when earth leakage from telephone wires caused a lot of crosstalk. Listening posts were established in order to intercept enemy messages. Next year valve amplifiers were utilised which allowed for extended listening range [5].

The US National Security Agency conducted classified research with codename TEMPEST in 1972 [6]. The document was later partially declassified

in 2007. It describes unwanted emanations coming from a Bell-telephone mixing device that was used for encryption. The signal allowed an attacker to reconstruct the original plain text. Researchers at Bell Lab demonstrated a practical attack from about 80 feet away that allowed reconstructing about 75% of the plain text being processed by the machine.

1.2 Related Work

Computer monitors started to become widespread in the end of the 20th century. Wim van Eck published the first unclassified technical analysis of the security risks of emanations from computer monitors in 1985 [2]. The next important publication regarding video emanations came from Markus Kuhn nearly 20 years later in 2003 [7]. Later in 2013, Elibol, Sarac and Erer demonstrated that emanations could be picked up from considerable distance with a mobile and lower cost equipment.

1.2.1 Work of Wim van Eck

Electromagnetic Radiation from Video Display Units: An Eavesdropping Risk? [2] was the first publicised research on the topic of emanations from video monitors. Wim van Eck describes the similarities between contemporary monitors and black and white TV sets. He explains that these could be exploited to build a cheap eavesdropping device.

The document describes conducting a practical attack with a modified black and white commercial television receiver. A demonstration is even done in real world conditions outside the laboratory. Van Eck proves that the attack is a viable security thread. He continues discussing possible sources of emissions and ways of defending against such attacks.

However, there are some problems with his implementation:

- The modification of the TV receiver, although inexpensive, requires advanced specialised knowledge to undertake.
- The fact that the device needs constant manual adjustments to keep the oscillators in the receiver and transmitter in sync makes it difficult to use in practice.
- Technology has changed dramatically since the publishing of the paper. The attack will no longer work on modern monitors due to the variety of video modes available which now differ significantly from broadcast television.
- No room for further automated signal processing.

We can only speculate why there was no further research on this topic for decades to come. Possibly the main reason was that a modified TV receiver will no longer work with modern day video modes and commercial off-the-shelf narrowband receivers can't be used for that purpose either. As Kuhn outlines, a researcher needed to have their hands on a very special military grade wideband receivers that are expensive and have export restrictions [7].

1.2.2 Work of Markus Kuhn

Markus Kuhn was able to improve on the results achieved by van Eck with his *Compromising emanations: eavesdropping risks of computer displays* [7]. In the technical report, Kuhn analyses the properties of the emitted waves and the possible emitting circuitry. He describes equipment an attacker may need in order to intercept and process the signal. He conducts experiments and constructs a system for real time monitoring using an FPGA board, a specialised wideband AM radio receiver and an off-the shelf VGA video monitor.

However, there are some limitations of Kuhn's real-time monitoring system:

- A researcher will need access to very expensive, export restricted equipment in order to repeat his experiments. This equipment also often

lacks the mobility required for a practical attack.

- As with van Eck system, Kuhn's solution still requires manual synchronisation.
- Digital signal processing for improving reception of weak signals (like time averaging) was not attempted in real time.
- An attacker will need to know the exact video parameters of the target or will need to guess them.

The report also mentions possible ways of modulating hidden messages into the signal. Kuhn discusses ways of defending against such attacks using hardware and software solutions. He demonstrates automatic character recognitions. The report includes experiments with optical eavesdropping of CRT displays.

Overall his real-time monitoring system improves on van Eck one by supporting a variety of modern video modes. Kuhn was able to prove that the threads outlined almost two centuries ago are still valid. This sparked fresh interest in the topic, resulting in a couple of additional related works to be published afterwards. In a later paper [8], Kuhn focuses on digital displays and explains that the same attack vector could also be used in that context. In [9] he analyses high frequency emissions from flat-panel LCD TV displays.

1.2.3 Work of Elibol et al.

In [10], Elibol, Sarac and Erer improve on the existing solution in that they demonstrate a cheaper and more mobile system that could be used to realistically eavesdrop a target. They demonstrate an attack from the considerable distance of 50 meters in real-time. They also mention an algorithm that uses autocorrelation to allow for interactively determining the horizontal synchronization frequency of the target display. Their implementation is the first that do not rely on synchronisation pulses to deconstruct the video image.

However:

- They did not attempt to reconstruct the vertical synchronisation frequency. This requires the attacker to have some prior knowledge of the target system.
- Their system is still not affordable, costing tens of thousands of pounds [11].

A research that followed by Ghani et al. [12] later focused on emissions from LCD touch screen displays of hand-held devices.

1.3 Achieved Goals and Motivation

The project aims to raise awareness of the potential security implications of the compromising emanations from video monitors. It implements the principles outlined in the related work section 1.2 using a completely new approach: utilising a software-defined radio receiver. It also combines them into a single portable software library. In its basic form it allows tuning to a video signal by manually controlling the video parameters, similar to the implementation that van Eck, Kuhn and Elibol et al. have used in their practical demonstrations.

The system builds on top of the existing research by having achieved the following additional goals that were never done before:

- Uses an affordable [2], unmodified off-the-shelf equipment portable enough to simplify practical attacks.
- Almost no specialised experience is necessary to operate the system.
- No prior knowledge of the target machine video parameters is required. The system can automatically estimate them remotely in real time.

[2] Costing only several hundred pounds [13].

- Reception of weaker signals is possible due to additional digital signal processing.
- Eliminates the need for constant manual adjustments in order to keep the picture steady on the screen.
- Open source license aiding further research on the topic.

The source code and the latest pre-compiled binaries could be obtained from github.com/martinmarinov/TempestSDR. If user's computer is running OS X, Windows or Linux, a multi-platform statically pre-compiled Java jar file is available for starting up the system in a couple of clicks. [3]

The system supports a plug-in architecture that allows simplified development of device drivers for any software-defined radio front-end. Currently supported plug-ins:

- Pre-recorded file with raw IQ samples (multi-platform support)
- Mirics SDR (Windows support)
- UHD (Linux and OS X support)
- ExtIO (Windows support)

The system comes with a Java GUI but the underlying library could be used independently by any other system as a shared or statically linked library. Furthermore the core is written in C and has no additional dependencies making it portable and easy to compile.

Chapter 2 provides some background information on the physics behind the radio wave generation process. It describes the basics of an SDR radio receiver. Chapter 3 explains the properties of the emanated signal and how to reconstruct it. It goes on describing the automatic remote estimation of video parameters. Chapter 4 demonstrates a practical attack, showing that an attacker, with no prior knowledge of the target video display, can use the

[3] Some device drivers might not be available on all operating systems. At time of writing the OS X binaries need to be compiled manually. Refer to the README for more information.

system to receive the compromising emanations from a distance. Chapter 5 outlines the architecture of the library and the implementation details. Finally, in chapter 6, a conclusion is done with some suggestions on further research.

However, the report does not discuss ways of limiting the amount of information leaked via such compromising emanations. This is beyond the scope of the project. The system could assist further research on the topic serving as a rapid prototyping tool.

The report also does not claim that the experimental results presented are exhaustive. This is due to the fact that there is a wide range of software-defined radio front-ends that are supported, each of them having different characteristics. Therefore no attempt was done to characterise the hardware used for the experiments. The presented measurements are not provided as absolute value (i.e. voltages) but rather as relative (i.e decibels). The results will very much depend on the target video display as well. Some displays will emit strong signals that could be picked up tens of meters away, while others emit no detectable video emanations. Characterising receivers and target video displays could be also left as a further research topic.

There are also some inherent notes about the system:

- The performance of the system depends on the speed of the CPU of the attacker. No GPU acceleration was implemented[4] since it wasn't really necessary. Performance never dropped below 40 fps on an Intel Core i5 laptop without GPU acceleration.
- Difficult to compare its core performance to existing implementations due to the fundamental differences of the underlying architectures.
- Software-defined radio receivers have a lower sensitivity and higher noise figure due to lack of high quality analogue filters compared to specialised wideband receivers. There is also interference caused by

[4]Some GPU acceleration may happen internally in the Java VM while resizing frames onto the screen.

their internal IC circuits or the USB/Ethernet/Power cables that connect them to the PC. However, Kuhn showed that in practice this could be greatly improved using suitable analogue preconditioning.

Chapter 2

Background

A reader should have knowledge of undergraduate level mathematics including calculus. Some equations and theorems are simply stated and then used. If the reader wants to learn more about their derivations, they need to look at a relevant textbook. Furthermore, it is assumed that the reader has a computer science background and understands the basic concepts behind object oriented programming and procedural programming. Familiarity with the C programming language and some basic knowledge of Java would be helpful as well. Understanding the basics of signal processing and Fourier theory is also desirable but not strictly required.

2.1 Signal Processing

The fact that changing currents in a wire induce currents in another nearby wire comes straight from Maxwell's equations [14]. A signal is just changing current and/or voltage in the time domain. Let's imagine we have a wire that we call wire A. We want to transmit a signal over it. We connect it to a signal generator that modulates some data $I(t)$, so that current across the wire at time t could be written as $x(t) = I(t)\sin(2\pi f_c t)$, where f_c is the carrier **frequency**. The argument of the sin, namely $2\pi f_c t$, is called the

phase of the wave. Because of Maxwell's equations, the changing current in wire A will also generate a circular changing magnetic field around itself.

Let's imagine that an adversary puts a wire B lying parallel to wire A. The changing magnetic field from wire A will generate a changing current in wire B. The adversary can measure the current in wire B as a function of time $\hat{x}(t)$. They will end up with $\hat{x}(t) = \hat{I}(f_c) \cdot I \cdot \sin(2\pi f_c t + \varphi(f_c))$ where $\hat{I}(f_c)$ is the attenuation of the peak amplitude and $\varphi(f_c)$ is the phase difference of the signal in wire B. Those particular values would depend on the physical properties of the system such as capacitance between the wires and their resistance. Having measured the carrier frequency f_c and by having some assumptions about the signal, an adversary could potentially make an estimate about $I(t)$. This is the source of the compromising emissions we observe – signals in wires unintentionally inducing currents in nearby wires, broadcasting some information about the original signal. In practice signals are more complex than just a single sin term, however Fourier analysis can help us.

The **Fourier transform** [15] allows us to see how the signal spectrum looks like in the frequency domain. This will decompose the function into a sum of sin and cos terms in the complex plane. The Fourier transform of $g(t)$ is defined as

$$G(f) = \mathcal{F}\left\{g(t)\right\}(f) = \int_{-\infty}^{\infty} g(t) \cdot e^{-2\pi j f t} \mathrm{d}t$$

and the inverse Fourier transform

$$g(t) = \mathcal{F}^{-1}\left\{G(f)\right\}(t) = \int_{-\infty}^{\infty} G(f) \cdot e^{2\pi j f t} \mathrm{d}f.$$

A sine wave of the form $x(t) = \sin(2\pi f_c t)$ will result in spikes $X(f) = \frac{1}{2i}[\delta(f - f_c) - \delta(f + f_c)]$ at $X(-f_c)$ and $X(f_c)$ since $X(f) = 0$ everywhere else. Therefore we can see that the Fourier transform basically gives an indication of the frequency of the source signal. Note that the **Dirac delta** function is defined as

$$\delta(t) = \begin{cases} +\infty, & x = 0 \\ 0, & x \neq 0 \end{cases}.$$

The Dirac delta functions have the so-called "sifting" property so that if multiplied with a function $g(t)$, it will **sample** out only a single value, namely

$$\int_{-\infty}^{\infty} g(t)\delta(t-T)\mathrm{d}t = g(T).$$

We will also encounter the "Dirac comb" defined as:

$$\text{Ш}_T(t) = \sum_{k=-\infty}^{\infty} \delta(t-kT) = \frac{1}{T}\text{Ш}\left(\frac{t}{T}\right)$$

which is basically an infinite number of Dirac delta functions repeating at regular intervals of T. We can therefore "sample" a function $x(t)$ at times T by multiplying it with a Dirac comb. This will result in discrete samples being obtained from $x(t)$ at regular intervals of T i.e. we will obtain $\ldots, x(-2T), x(-T), x(0), x(T), x(2T), \ldots$.

We also need to mention **convolution**, denoted by the operator $*$. The convolution of two functions $x(t)$ and $g(t)$ is defined as

$$(f * g)(t) = \int_{-\infty}^{\infty} f(\tau)g(t-\tau)\mathrm{d}\tau.$$

To illustrate how convolution works, consider convolving a function $x(t)$ with a Dirac delta

$$\big(\{x(t)\} * \{\delta(t-T)\}\big)(t) = \int_{-\infty}^{\infty} x(\tau)\delta(t-\tau-T)\mathrm{d}\tau = \int_{-\infty}^{\infty} x(\tau)\delta(\tau-(t-T))\mathrm{d}\tau = x(t-T) \quad (2.1)$$

where we used the fact that the Dirac delta function has an even symmetry $\delta(t) = \delta(-t)$. This results in a new function $x(t-T)$ which is a time shifted copy of $x(t)$ with a shift of T. Convolving with a Dirac comb could be shown to produce infinite copies of $x(t)$ at regular intervals T which are basically summed together.

The term **low-pass** means a low-pass filter. This is a filter that acts on a

signal, and that allows components of the signal with frequencies $f \leq f_{\max}$ to pass through, attenuating the rest to 0. A **high-pass** filter allows frequencies $f \geq f_{\min}$ to pass through intact, attenuating the rest to 0. A **band-pass** filter is a combination of a low-pass and a high-pass filter, allowing only frequencies $f_{\min} \leq f \leq f_{\max}$, attenuating the rest to 0. A **band-limited** signal is a signal which doesn't have any frequency components $f > f_{\max}$ or $f < f_{\min}$. Such a signal would remain unchanged after applying a band-pass filter to it with limits $f_{\min}$ and $f_{\max}$. This is used for filtering out useful signals from other interferences that are not part of the band-limited signal.

2.2 IQ Sampling

A simple analogue to digital converter will measure the voltage in a wire by producing f_{s} samples per second (called **sampling rate**). This means that it will produce a new sample every $t_{\mathrm{s}} = \frac{1}{f_{\mathrm{s}}}$ seconds. It converts an analogue signal a.k.a. continuous function $x(t)$ into a series of samples. This could be written mathematically as a multiplication with a Dirac comb

$$\hat{x}(t) = \sum_{k=-\infty}^{\infty} x(t)\delta(t - kT). \tag{2.2}$$

If we want to detect a signal containing frequency components from 0 up to $f_{\max}$, then according to the Nyquist sampling theorem, we need to sample with a sample rate $f_{\mathrm{s}} > 2f_{\max}$. This usually gets impractical when $f_{\max}$ gets large.

However, if we are only interested in a band-limited signal that lies from $f_{\min}$ up to $f_{\max}$, there is another solution. We can have a local oscillator that runs at a frequency $f_{\mathrm{LO}} = \frac{f_{\min}+f_{\max}}{2}$. The oscillator generates a signal $A_{\mathrm{LO}} \cdot \cos(2\pi f_{\mathrm{LO}} t)$. The output from the local oscillator is multiplied with the incoming **RF** (radio frequency) baseband signal (a.k.a. mixing). Say the RF signal is $x(t) = A(t)\cos(2\pi f_{\mathrm{c}} t)$. It has a frequency of f_{c} and phase of $2\pi f_{\mathrm{c}} t$. For simplicity, let's put $A_{\mathrm{LO}} = 2$. After the mixing stage, our resulting signal

will be

$$x(t) \cdot A_{\mathrm{LO}} \cos(2\pi f_{\mathrm{LO}} t) = A(t)\cos(2\pi f_{\mathrm{c}} t) \cdot 2\cos(2\pi f_{\mathrm{LO}} t) = \\ = A(t)\cos\big(2\pi(f_{\mathrm{c}} + f_{\mathrm{LO}})t\big) + A(t)\cos\big(2\pi(f_{\mathrm{c}} - f_{\mathrm{LO}})t\big). \quad (2.3)$$

This results in a linear combination of two signals with frequencies called heterodyne frequencies – the sum and the difference between the local oscillator and the incoming frequency. A band-pass filter could be set up at an **IF** (intermediate frequency) f_{IF}. If any of these heterodyne frequencies falls within the band-pass of the filter, the signal can go for further processing.

However, we encounter a problem: cos is an even function. Imagine we now have another RF baseband signal, namely $\hat{x}(t) = A(t)\cos\big(2\pi(2f_{\mathrm{LO}} - f_{\mathrm{c}})t\big)$. After mixing with the local oscillator, the resulting signal would be $A(t)\cos\big(2\pi(f_{\mathrm{LO}} - f_{\mathrm{c}})t\big)$ which is equivalent to what we obtained for $x(t)$ in (2.3) for the difference $f_{\mathrm{LO}} - f_{\mathrm{c}}$ signal. So we can't distinguish $\hat{x}(t)$ from $x(t)$ if we decide to only filter out the difference part. This is called signal imaging. It could be shown that a signal $\tilde{x}(t) = A(t)\cos\big(2\pi(-f_{\mathrm{c}} - 2f_{\mathrm{LO}})t\big)$ will in turn generate a sum $A(t)\cos\big(2\pi(-f_{\mathrm{LO}} - f_{\mathrm{c}})t\big)$ which again results in imaging if we decide to keep the summation term $f_{\mathrm{LO}} + f_{\mathrm{c}}$ from (2.3).

This method can preserve the amplitude of the wave and is widely used in AM radio reception (in conjunction with some image rejection techniques as well). However, it is obvious from the problem outlined above that the method is not sufficient for uniquely detecting the phase of the incoming wave. A solution to this problem is to multiply the incoming RF signal with a phase shifted version of the local oscillator at an angle of 90° in parallel with the mixing from (2.3). This means multiplying by $-A_{\mathrm{LO}} \cdot \sin(2\pi f_{\mathrm{LO}} t)$. After this secondary mixing stage, we would get

$$-x(t) \cdot A_{\mathrm{LO}} \sin(2\pi f_{\mathrm{LO}} t) = -A(t)\cos(2\pi f_{\mathrm{c}} t) \cdot 2\sin(2\pi f_{\mathrm{LO}} t) = \\ = -A(t)\sin\big(2\pi(f_{\mathrm{c}} + f_{\mathrm{LO}})t\big) + A(t)\sin\big(2\pi(f_{\mathrm{c}} - f_{\mathrm{LO}})t\big). \quad (2.4)$$

Now let's put $\varphi(t) = 2\pi(f_{\mathrm{c}} - f_{\mathrm{LO}})t$, and we only take the terms that contain

φ in (2.3) and (2.4), namely the difference terms using a band-pass filter of width $\frac{f_\mathrm{s}}{2}$. Then we can define

$$I(t) = A(t)\cos(\varphi(t)) \quad \text{and} \quad Q(t) = A(t)\sin(\varphi(t)). \tag{2.5}$$

Sampling these continuous signals with an analogue to digital converter will result in discrete values at times t_{f_s}. Let's put $A_n = A(nt_\mathrm{s})$ and $\varphi_n = \varphi(nt_\mathrm{s})$. Then we can define our resulting discrete samples as

$$I_n = A_n\cos(\varphi_n) \quad \text{and} \quad Q_n = A_n\sin(\varphi_n). \tag{2.6}$$

These I and Q samples form the basic principles of software-defined radio. I and Q stand for in-phase and quadrature phase [16]. These terms refer to the cos and $-\sin$ oscillator phases used for mixing. After the IQ samples are obtained, they are received by a PC with a sample rate of f_s.

IQ sampling allows monitoring frequencies from $-\frac{f_\mathrm{s}}{2}$ to $\frac{f_\mathrm{s}}{2}$. To compare, normal sampling would only allow a maximum frequency span from 0 to $\frac{f_\mathrm{s}}{2}$ since signals are only sampled with real values (Nyquist theorem). This would cause the imaging we discussed before. IQ sampling improves on the simple Nyquist sampling using complex numbers – effectively doubling the range.

Once IQ samples are obtained by software, further analysis of their phase, frequency and amplitude could be done. This would allow any signal that is band-limited from $-\frac{f_\mathrm{s}}{2}$ to $\frac{f_\mathrm{s}}{2}$ to be represented without aliasing. The following identities relate the amplitude A_n, frequency ω_n, and phase φ_n of a sample n

$$A_n = \sqrt{I_n^2 + Q_n^2} = \sqrt{A_n^2 \cdot (\cos^2(\varphi_n) + \sin^2(\varphi_n))} \tag{2.7a}$$

$$\varphi_n = \tan^{-1}\left(\frac{Q_n}{I_n}\right) = \tan^{-1}\left(\frac{\sin(\varphi_n)}{\cos(\varphi_n)}\right) \tag{2.7b}$$

$$\omega_n = \frac{\mathrm{d}\varphi_n}{\mathrm{d}t} = \varphi_n - \varphi_{n-1}. \tag{2.7c}$$

Refer to Figure 2.1 for geometrical representation of the outlined properties.

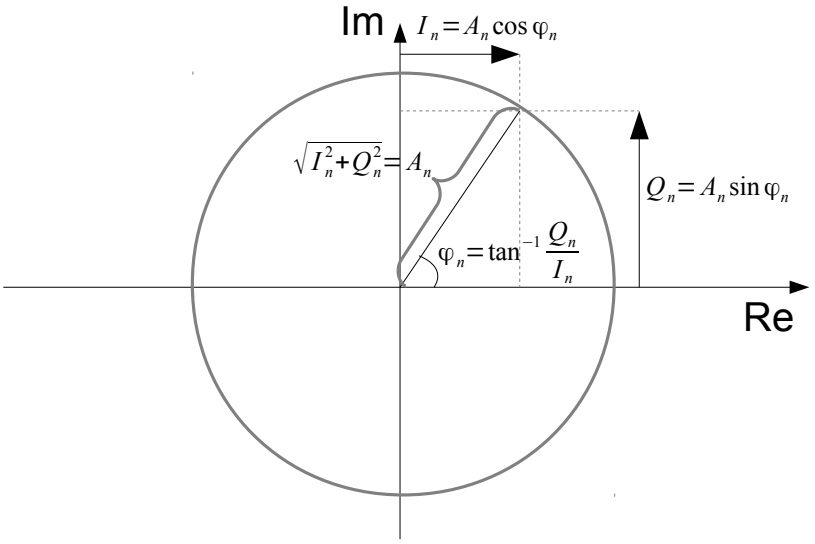

Figure 2.1: Graphical representation of an IQ sample n in the complex plane. All points with the same amplitude A_n will lie on the circle showed in gray. The angle that the sample vector makes with the real axis is the instantaneous phase φ of the sample.

Chapter 3

Methodology

3.1 Analogue Video Signals

Almost all contemporary video monitors are raster based. The image is transferred from the video controller to the display in scan lines that occur at a specific rate. Each of these scan lines contains a number of pixels which are continuously encoded as a time varying signal. This signal is generated internally in the video controller by an oscillator which runs at the pixel clock rate. The analogue signal is thereafter multiplied by the pixel intensities at the specific time.

Let's assume that the signal started transmitting at time $t = 0$, and each video frame contains y_t scanlines, each of which contains x_t pixels. The frequency with which frames are being generated is f_v frames per second. The duration of transmission of each individual pixel is

$$t_\mathrm{p} = \frac{1}{x_\mathrm{t} \cdot y_\mathrm{t} \cdot f_\mathrm{v}}. \tag{3.1}$$

Note that at time t, frame number $n(t)$ started transmission where

$$n(t) = \lfloor t f_\mathrm{v} \rfloor. \tag{3.2}$$

We can assume that the top left corner of a frame has coordinates $(0, 0)$, a pixel at position (x, y) in frame $n(t)$ will start to be transmitted at time

$$T_{(x,y)} = (n(t)x_{\mathrm{t}}y_{\mathrm{t}} + yx_{\mathrm{t}} + x)t_{\mathrm{p}} \tag{3.3}$$

and will finish transmission before time

$$T_{(x+1,y)} = T_{(x,y)} + t_{\mathrm{p}} = (n(t)x_{\mathrm{t}}y_{\mathrm{t}} + yx_{\mathrm{t}} + x + 1)t_{\mathrm{p}} \tag{3.4}$$

at which the next pixel will start transmitting.

In practice x_{t} and y_{t} are determined by the screen resolution and f_{v} is simply the screen refresh rate. For a typical screen resolution of $width \times height$, it is true that $x_{\mathrm{t}} \geq width$ and $y_{\mathrm{t}} \geq height$. The reason is that video signals tend to have additional blanking intervals. This means more pixels are transmitted than what is in the active video region. This gives opportunity for the receiving monitor to synchronise its internal oscillator, calibrate its colour levels, or in case of CRT, allow enough time for the electron beam to return to the beginning of the next line on the screen. The synchronisation timings for personal computers have been standardised by Video Electronics Standards Association (VESA) [17].

In order to decode an individual pixel, the receiving monitor has its own internal oscillator. It locks it to the pixel rate of the incoming signal either via an external clock source or using the blanking intervals. Once it receives the signal for an individual pixel, its amplitude (or binary content in case of digital signal) will correspond to the intensity. This allows the monitor to display the video in real time. If multiple colours are desired, they can be transmitted separately on different wires in the same fashion.

3.2 Generated Radio Wave

3.2.1 Analogue Video Signal Equation

Let's assume the discrete pixels in an analogue video signal have intensities v_i ($i \in \mathbb{Z}$) and are being transmitted for duration $t_\mathrm{p} = \frac{1}{x_\mathrm{t} \cdot y_\mathrm{t} \cdot f_\mathrm{v}}$ from (3.1). Let's also assume that the shape of the pixel is $p(t)$ where $p(t) = 0$ for $|t| \gg \frac{t_\mathrm{p}}{2}$. We know that pixel i starts transmitting at time $t_i = it_\mathrm{p}$ (if we assume that that pixel 0 was transmitted at $t = 0$). Also the amplitude of the signal of the transmitted pixel is linearly dependant on its intensity v_i. Then the resulting video signal in the time domain will have the form

$$\tilde{v}(t) = \sum_{i=-\infty}^{\infty} v_i p(t - it_\mathrm{p}) \tag{3.5}$$

which is a continuous function. (3.5) can be rewritten as a convolution with a Dirac delta function

$$\tilde{v}(t) = p(t) * \left(\sum_{i=-\infty}^{\infty} v_i \cdot \delta(t - it_\mathrm{p}) \right) = p(t) * \hat{v}(t) \tag{3.6}$$

where

$$\hat{v}(t) = \sum_{i=-\infty}^{\infty} v_i \cdot \delta(t - it_\mathrm{p}). \tag{3.7}$$

Note that this results in infinitesimally short (in time) spikes at values exact integer multiples of t_p with amplitudes weighted to the pixel intensities at that time. We can view (3.6) as the pixel shape being repeated at intervals of t_p modulated by v_i.

3.2.2 Sampling

Note that (3.7) looks like the result of a continuous signal being sampled at discrete points in time t_p apart. If we call this hypothetical continuous signal

$v(t)$, then we can rewrite the equation so that it reads

$$\hat{v}(t) = \sum_{i=-\infty}^{\infty} v(t) \cdot \delta(t - it_{\mathrm{p}}) = v(t) \sum_{i=-\infty}^{\infty} \delta(t - it_{\mathrm{p}}) = v(t) \cdot \text{Ш}_{t_p}(t). \quad (3.8)$$

The requirement is that if $v(t)$ is sampled at discrete intervals it_{p}, it should be equal to the corresponding pixel values i.e. $v(0) = v_0$, $v(t_{\mathrm{p}}) = v_1$, $v(2t_{\mathrm{p}}) = v_2$, etc. This would mean that we can precisely obtain the samples from the continuous function by applying the series of Dirac delta functions. However, now we would also like to be able to obtain the continuous signal by only having the sampled values v_i. This means that we need a unique perfect reconstruction i.e. to be able to obtain all v_i from $v(t)$ and $v(t)$ from all v_i. Under the assumption that $v(t)$ is band-limited so that $\mathcal{F}\big(v(t)\big)(f) = 0$ for $|f| < \frac{t_{\mathrm{p}}}{2}$, the condition is satisfied by the Whittaker–Shannon interpolation formula [18]. It states that the continuous signal could be uniquely reconstructed using sinc interpolation. If we apply it to our v_i samples, it yields

$$v(t) = \sum_{k=-\infty}^{\infty} v_k \cdot \mathrm{sinc}\left(\frac{t}{t_{\mathrm{p}}} - k\right) \quad (3.9)$$

where we use the definition $\mathrm{sinc}(x) = \frac{\sin(\pi x)}{\pi x}$ .We can verify that when $t = it_{\mathrm{p}}$, then $\mathrm{sinc}(i - k)$ will always yield 0 except for when $i = k$ in which case it will be 1. Therefore we have proved that $v(it_{\mathrm{p}}) = v_i$.

3.2.3 Spectrum Repetitions

Now let's revise some mathematical identities. According to the convolution theorem [19]

$$\mathcal{F}\{g \cdot h\} = \mathcal{F}\{g\} * \mathcal{F}\{h\} \quad (3.10)$$

which reads: the Fourier transform of a multiplication of two functions is equivalent to the Fourier transforms of the individual functions convolved

together. And vice versa

$$\mathcal{F}\{g * h\} = \mathcal{F}\{g\} \cdot \mathcal{F}\{h\}, \tag{3.11}$$

the convolution of the Fourier transform of two functions is equivalent to the individual Fourier transforms of the two functions multiplied together. It could be also shown that

$$\mathcal{F}\{\text{Ш}_k(t)\} = \mathcal{F}\left\{\sum_{n=-\infty}^{\infty} \delta(t - nk)\right\} = k^{-1} \sum_{n=-\infty}^{\infty} \delta\left(t - k^{-1}n\right) = k^{-1}\text{Ш}_{k^{-1}}(t) \tag{3.12}$$

using the last three identities, we can write the Fourier transform of (3.6) as

$$\tilde{V}(f) = \mathcal{F}\{p(t) * \hat{v}(t)\} = \mathcal{F}\left\{p(t) * \left(v(t) \cdot \text{Ш}_{t_p}(t)\right)\right\} = \frac{1}{t_\text{p}} P(f) \cdot \left[V(f) * \text{Ш}_{t_p^{-1}}(f)\right] \tag{3.13}$$

where $P(f)$ is the Fourier transform of $p(t)$, $\tilde{V}(f)$ is the Fourier transform of $\tilde{v}(t)$ and $V(f)$ is the Fourier transform of $v(t)$. This simply means that the signal spectrum $V(f)$ repeats at regular intervals throughout the radio spectrum with a frequency of $\frac{1}{t_\text{p}} = x_\text{t} \cdot y_\text{t} \cdot f_\text{v}$. The intensities of the emission at the different frequencies is determined by the shape of the pixel $p(t)$.

For example, for a resolution of 800×600 @ 75 fps with $x_\text{t} = 1056$ px, $y_\text{t} = 628$ lines and $f_\text{v} = 75$ Hz , we would have a frequency of $\frac{1}{t_\text{p}} = 1056 \times 628 \times 75 \simeq 49.74$ MHz. This means that we would expect to find such a signal centred at DC, 49.74 MHz, 99.48 MHz, 149.2 MHz, etc.

In order to obtain the full video signal, we need to know what is the minimum rate at which we need to sample the baseband. We saw from (3.13) that $V(f)$ repeats at the regular intervals. As a consequence from the Whittaker–Shannon interpolation formula that we used to construct $v(t)$, we know that $V(f)$ is band limited so that $V(f) = 0$ for all $|f| \geq \frac{1}{2t_\text{p}}$. Therefore we need to have a receiver with a sampling rate of at least $\frac{1}{t_\text{p}}$.

These findings agree with the results that Markus Kuhn obtained in his

analysis of the emanated signal who used a slightly different approach to derive them [7].

3.2.4 Digital Video Signal Equation

The analysis above was aimed at analogue signals such as the ones transmitted via VGA. However the majority of contemporary laptops and similar devices don't simply modulate the pixel intensities as analogue voltage amplitudes. Instead, they send each pixel as digital bits using FPD-Link (Flat Panel Display Link) to transmit LVDS (Low-voltage differential signalling). For each pixel, 7 bits are transmitted over each of the three wires that determine the resulting RGB colour.

Therefore each bit is transmitted for a duration of $t_\mathrm{b} = \frac{1}{x_\mathrm{t} \cdot y_\mathrm{t} \cdot f_\mathrm{v} \cdot n_\mathrm{b}} = \frac{t_\mathrm{p}}{n_\mathrm{b}}$ where n_b is the number of bits per pixel which in case of FPD-Link is $n_\mathrm{b} = 7$. This represents a bit stream of values c_k ($k \in \mathbb{Z}$). We defined the k-th value being the ($k \mod n_\mathrm{b}$) bit of the binary number that is used to represent the analogue pixel intensity of pixel number $\left\| \frac{k}{n_\mathrm{b}} \right\|$ (remember, the intensity of pixel number i is denoted as v_i).

Therefore, we can write the resulting analogue signal as

$$\tilde{v}(t) = \sum_{k=-\infty}^{\infty} c_k b(t - k t_\mathrm{b})$$

where $b(t)$ is the shape of a digital bit where $b(t) = 0$ for $|t| \gg \frac{t_\mathrm{b}}{2}$.

Now assuming $c(t)$ is the continuous version of c_k as in the previous section, we can do the same Fourier analysis on this signal, similar to (3.13) to obtain

$$\mathcal{F}\left\{ b(t) * \left(c(t) \cdot \text{Ш}_{t_b}(t) \right) \right\} = \frac{1}{t_\mathrm{b}} B(f) \cdot \left[C(f) * \text{Ш}_{t_b^{-1}}(f) \right]. \tag{3.14}$$

This means that we will also get repeating signal throughout the spectrum, this time repeating with a frequency of $\frac{1}{t_\mathrm{b}} = x_\mathrm{t} \cdot y_\mathrm{t} \cdot f_\mathrm{v} \cdot n_\mathrm{b}$. This is n_b times higher than the calculated repetition frequency for analogue signals.

For example, Markus Kuhn's laptop was running LVDS with $n_\mathrm{b} = 7$ at a video mode of 800×600 @ 75 with $x_\mathrm{t} = 1056$ px, $y_\mathrm{t} = 628$ lines and $f_\mathrm{v} = 75$ Hz. He reports receiving a harmonic emanation at about 350 MHz[1] [8]. We can see that this agrees with the theoretical predictions since for his case $\frac{1}{t_\mathrm{b}} = 1056 \cdot 628 \cdot 75 \cdot 7 \simeq 348.2$ MHz.

However, the signal is now wider. We would need a receiver that can pick up $|f| \geq \frac{1}{2t_\mathrm{b}} \equiv \frac{n_\mathrm{b}}{2t_\mathrm{p}}$ in order to reconstruct individual bits. In practice, we can still use the same approach that we used for analogue video. We can have a receiver that can pick up $|f| \geq \frac{1}{2t_\mathrm{b}}$. This is essentially equivalent to applying a low-pass filter – we will no longer be able to distinguish individual bits. Instead we will obtain an averaged out value for each pixel that depends on the underlying binary data that is used to represent its intensity. The variety of colours available with significantly different bit patterns means that we can still extract a lot of visual information from the reconstructed image.

3.3 Reception

3.3.1 Theory

Firstly, in order to receive a copy of the video signal, we will need to apply a band-pass filter centred at a multiple of the pixel frequency. The width of the band-pass needs to be the same as the band limited video signal we want to eavesdrop. Secondly, we need to generate an internal clock that runs at the pixel rate and use that to obtain the estimated pixel intensities. Luckily the first step can be done by an AM (Amplitude Modulation) receiver. Unfortunately the signal bandwidth is much wider than what a typical off-the-shelf AM receiver can handle.

However some software-defined radio receivers can provide the required band-

[1] His actual hardware is transmitting two pixels at a time, resulting in a factor of $\frac{1}{2}$ being applied to the end result. Therefore the first harmonic he could actually pick up lies at 175 MHz.

width. The Ettus Research USRP B200 can provide more than 50 MHz of real-time bandwidth which covers what is required to eavesdrop most video signals. Software-defined radios provide the radio samples as a quadrature vector which angle relates to the instantaneous phase in relation to the internal hardware oscillator of the hardware. The size of the vector is proportional to the received amplitude for each sample (refer to Section 2.2 for more information). For AM reception, we do not need the phase information since the video signal is being transmitted with a constant frequency. Therefore we can make a simple AM demodulator by taking the length of the vector of each sample. When our digital sampling rate matches the pixel rate, each sample will contain an estimate that relates to the average pixel intensity between time t_i and t_{i+1}. For digital signals, it would be related to the bit pattern of the binary value (although this relation may not be unique) that represents the intensity for the current pixel.

3.3.2 Practice

The VESA standard specifies an allowed frequency tolerance for f_{v} of 0.5%. Therefore due to hardware limitations, we might not be able to accurately tune the receiver sampling rate with enough accuracy to match the transmitted pixel rate. This means that some re-sampling needs to be done in software in order to create a new digital signal that matches as close as possible the transmitted pixel rate in which each sample corresponds to a pixel.

It is also true that we might be able to recover a lot of information from a signal even if our receiver is not capable of sampling the full width of the video spectrum. This means we will only receive $v(f)$ with a band-pass filter applied to it. In this case the digital re-sampling could interpolate the received samples to fit into multiple pixels. Therefore it is useful to introduce a measurement κ of how accurate we can reconstruct pixels of $v(t)$. This measurement can be the number of input samples that have gone

into constructing a single output pixels. Therefore

$$\kappa = f_{\mathrm{s}} \cdot t_{\mathrm{p}} = \frac{f_{\mathrm{s}}}{x_{\mathrm{t}} \cdot y_{\mathrm{t}} \cdot f_{\mathrm{v}}} \tag{3.15}$$

whereas before, f_{s} is the receiver sampling rate. If $\kappa \geq 1$, then we can deconstruct individual pixels. If $\kappa < 1$ we are looking at a band-passed version of the signal and consecutive reconstructed pixels will have some interdependencies. Please refer to Figure 3.1 for a visual comparison of different values of κ.

Another possible source of distortions is the usage of multiple wires to transmit colour information. These signals interfere with each other and the resulting pixel intensity becomes a complicated mix of the signals generated in these wires. Therefore colour information would be very difficult to obtain. Nevertheless the outlined strategy allows an eavesdropper to detect changes in colour since this would result in different signal amplitudes arriving at the receiver for each pixel.

3.4 Resolution and Frame Rate Detection

The outlined method for decoding the video stream relies on us having the exact values for x_{t}, y_{t} and f_{v}. This is not very practical for a real world attack. We would require the adversary not to have any knowledge of the target system whatsoever. Therefore we would need to infer all these parameters remotely by exploiting some typical characteristics of a video signal. Namely the fact that the signal is periodic.

As we have already seen, a video signal consists of video frames with width x_{t} and height y_{t}. The speed at which such frames are transmitted is f_{v}. However most of the time any two consecutive frames would be identical. This would be the case if the victim is looking at static text on the screen. Therefore we can regard the transmitted signal as a repeating periodic signal of a single frame. Which means if we analyse the signal for repeating patterns

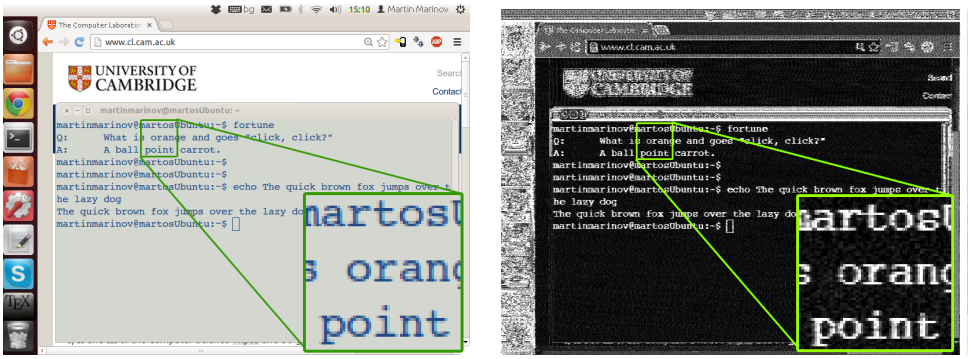

(a) Transmitted image

(b) $\kappa = 1.003$

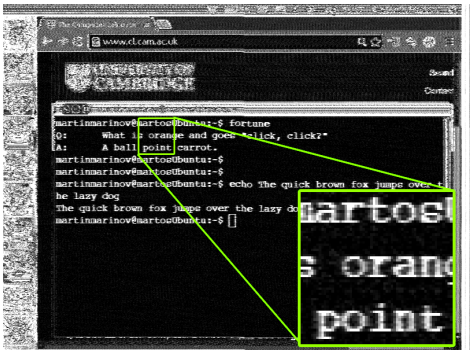

(c) $\kappa = 0.753$

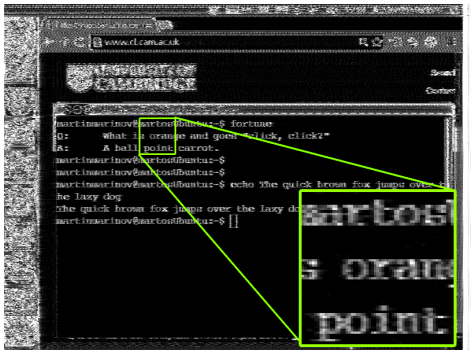

(d) $\kappa = 0.502$

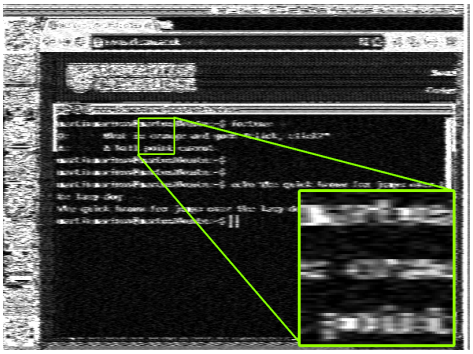

(e) $\kappa = 0.251$

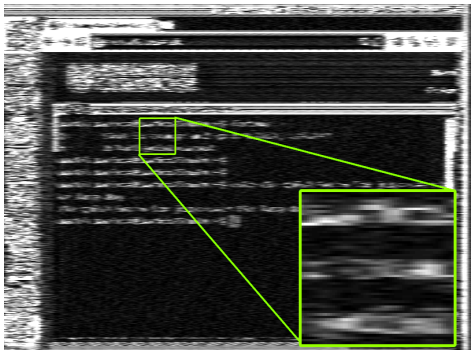

(f) $\kappa = 0.125$

Figure 3.1: The transmitted image (a) is sent via a standard HDMI to VGA converter. The emanations are coming from the digital video signal. The resolution is 800×600 @ 60 with $x_\mathrm{t} = 1056$, $y_\mathrm{t} = 628$ and $f_\mathrm{v} = 60.11$. Each of the following screen shots represent an eavesdropped version from a distance of 1 m with the receiver (USRP B200) running at different sample rates: (b) 40 MHz, (c) 30 MHz, (d) 20 MHz, (e) 10 MHz and (f) 5 MHz

we should be able to spot the repeating video frames in it and use that to estimate f_{v}.

3.4.1 Introduction to Autocorrelation

A good way of estimating f_{v}, would be by calculating the discrete autocorrelation [20] of the incoming signal which is defined as

$$R_{vv}(j) = \sum_{i=-\infty}^{\infty} v_i \bar{v}_{i-j} \tag{3.16}$$

where $\bar{v}$ is the complex conjugate of v and j is the **samples lag**. In our case v is the set of real samples, therefore $\bar{v} = v$. Basically the autocorrelation is a measure of the similarity of a signal with itself shifted by a lag. The higher the value of $R_{vv}(j)$ is, the more similar the function is at that lag. Therefore by analysing $R_{vv}(j)$, we would be able to spot any repeating patterns inside v_i.

Figure 3.2 shows the discrete autocorrelation $R_{vv}(j)$ of a video signal that was captured using the Mirics USB dongle at 8 MHz (i.e. $8,000,000$ samples per second) sampling rate. The vertical axis is logarithmic, containing the decibels of the autocorrelation i.e. $10\log_{10}(R_{vv})$. The horizontal axis contains the time lag in milliseconds. This was converted from the lag in samples j by $x = \frac{j}{f_{\mathrm{s}}}$.

The particular example consists of $524,288$ samples which is 65.536 milliseconds of recording. This allows us to estimate the autocorrelation up to half of it, namely 32.768 milliseconds. The reason is that $R_{vv}(j) = -R_{vv}(j)$ due to symmetry. We can see a peak at 16.672 milliseconds which corresponds to a frequency of $f_{\mathrm{v}} = \frac{1}{0.016672} = 59.98$ Hz. This is our estimate for f_{v}. And it makes sense, 60 Hz is a common refresh rate for contemporary video displays.

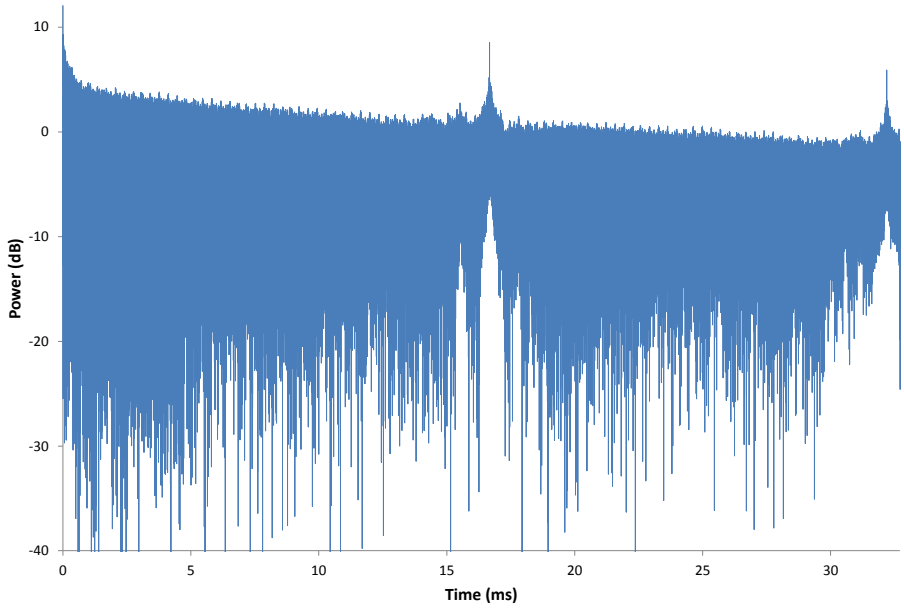

Figure 3.2: Autocorrelation of a signal

3.4.2 Aliasing

We should be able to see the peak repeating at $2 \times 16.672 = 33.344$ ms. This is analogous to comparing every two consecutive frames with every two other frames. However, as this falls just outside our window, $33.344 > 32.768$, it would be seen as an alias at $65.536 - 33.344 = 32.192$ ms. The same applies for the third peak at $3 \times 16.672 = 50.016$ ms which would be comparing each block of three consecutive frames with the next three. This will alias at $65.536 - 50.016 = 15.52$ ms. This explains the second small peak we see on the left of the main one at 16.672 ms but we see that the difference in its power is already several decibels lower. Therefore any further aliasing induced would be even smaller.

It is therefore important to choose the number of samples to be used for the autocorrelation wisely in order to avoid aliasing. We need to have enough full frames in our data so that the autocorrelation can physically work. The

minimum frequency we can get from an autocorrelation is $\frac{2s}{N}$ where N is the total number of samples that we are doing the autocorrelation on. It could be easily shown that the second alias is

$$\hat{f}_2(f) = \frac{1}{\frac{2}{f_{\min}} - \frac{2}{f}} = \frac{1}{\frac{N}{f_s} - \frac{2}{f}} \tag{3.17}$$

where f is the frequency we are going to see the alias for. Therefore if we want to be able to pick up a repeating pattern of at least $f_{\min} = 50$ Hz, we would need $\frac{2s}{50}$ which in our case is $320,000$ samples. However having such few samples, if we observe a signal at 85 Hz, we would discover a strong alias at $\left(\frac{320{,}000}{8{,}000{,}000} - \frac{2}{85}\right)^{-1} = 60.714$ Hz which would be very misleading and will look like a legitimate signal at 60.714 Hz.

Let us assume $f_{\text{low}} \leq f_{\text{v}} \leq f_{\text{hi}}$. In order to minimise aliasing, we can try to keep the second alias $\hat{f}_2(f_{\text{src}})$ outside this range. Therefore we need to pick the number of samples so that

$$f_{\text{low}} \geq \hat{f}_2(f_{\text{low}}) \equiv \frac{1}{\frac{N}{f_s} - \frac{2}{f_{\text{low}}}} \quad \text{or} \quad f_{\text{hi}} \leq \hat{f}_2(f_{\text{hi}}) \equiv \frac{1}{\frac{N}{f_s} - \frac{2}{f_{\text{hi}}}}$$

which means that

$$N \geq 3\frac{f_s}{f_{\text{low}}} \quad \text{or} \quad N \leq 3\frac{f_s}{f_{\text{hi}}}$$

and don't forget that in the same time we have the condition

$$N \geq 2\frac{f_s}{f_{\text{low}}}$$

so in the end, in order to eliminate the second alias in the desired region from f_{low} to f_{hi} in the autocorrelation, we would need to choose the number of samples to be

$$N \geq 3\frac{f_s}{f_{\text{low}}}. \tag{3.18}$$

To paraphrase this result, we will need to do the autocorrelation on at least 3 frames worth of samples for the lowest frequency in our range f_{low} to avoid second order aliasing interfering with our plot.

3.4.3 Number of Lines in a Frame

We were able to estimate f_{v} using an autocorrelation and eliminate aliased signals in the frequency window that we are looking to detect repetitions. However, we still have not estimated neither x_{t}, nor y_{t}. As a matter of fact we might not be able to measure x_{t} at all. The reason is that x_{t} might be a continuous signal and could potentially contain any number of pixels. However, each line of x_{t} pixels repeat y_{t} times in a frame which includes the blanking intervals. Therefore we can use the repeating nature of the blanking intervals to estimate y_{t} from the autocorrelation plot.

For this reason we need to zoom in to our plot. Refer to Figure 3.3 which is a zoomed out version of the figure we saw in the previous subsection. If we still have our allowed f_{v} window between f_{low} and f_{hi}, then we can assume that y_{t} also spans between h_{low} and h_{hi}. We would therefore expect to see a peak between $\frac{1}{f_{\mathrm{hi}} \cdot h_{\mathrm{hi}}}$ and $\frac{1}{f_{\mathrm{low}} \cdot h_{\mathrm{low}}}$ milliseconds. If we detect a peak at time t_{peak}, then this would correspond to $y_{\mathrm{t}} = \left\| \frac{1}{t_{\mathrm{peak}} \cdot f_{\mathrm{v}}} \right\|$ where $\|$ represents rounding to the nearest integer. Note that we should have already estimated f_{v}.

Our plot shows a peak at 0.017875 milliseconds. Since we already estimated $f_{\mathrm{v}} = 59.98$ Hz, then $y_{\mathrm{t}} = \left\| \frac{1000}{0.017875 \times 59.98} \right\| = 933$ lines. If we look at a list of VESA video modes, we can see that there is a conveniently close video mode that corresponds to $y_{\mathrm{t}} = 933$ and $f_{\mathrm{v}} = 59.98$. It is the 1440×900 @ 60 video mode with $x_{\mathrm{t}} = 1904$ pixels, $y_{\mathrm{t}} = 932$ lines and $f_{\mathrm{v}} = 60$ Hz. Therefore we could use the value of $x_{\mathrm{t}} = 1904$ for our estimate of the number of pixels in a row. This will keep the aspect ratio correct.

We should not worry about aliasing since the number of samples in the autocorrelation is much bigger than our range. We can see on the plot the autocorrelation values repeating for each two lines, each three lines, etc. This results in a number of peaks repeating with the rate at which individual lines repeat in the video signal.

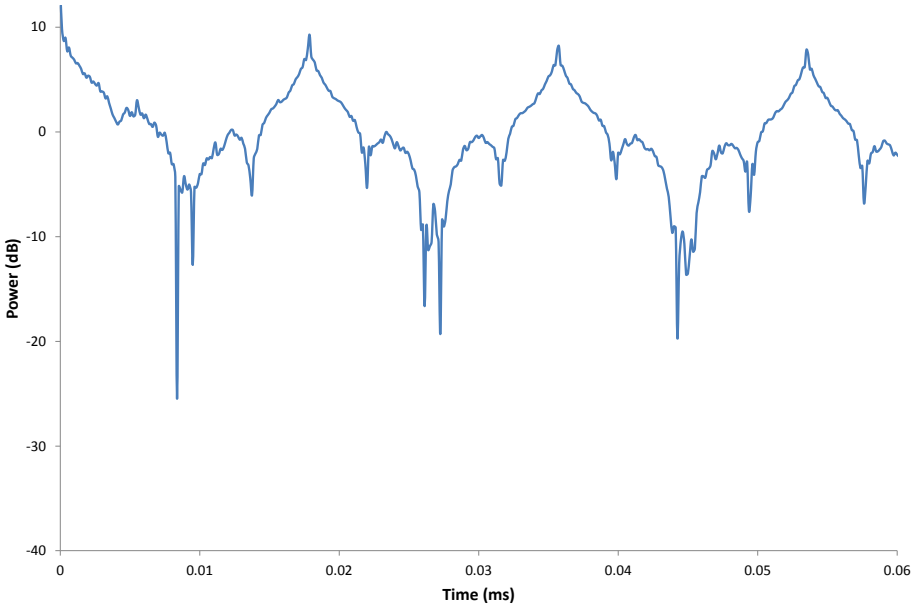

Figure 3.3: Zoomed in version of 3.2

3.4.4 Errors

There is a limit on how accurately one can determine f_{v} and y_{t} using the outlined autocorrelation method. This depends on the sampling rate of the device. The resolution of the autocorrelation is $\delta f = \frac{1}{f_{\mathrm{s}}}$. Therefore we can only say that if there is a peak at t_x in the autocorrelation, then we have a repeating component in the signal with a frequency $f_x \pm \delta f$.

The accuracy at which we can determine y_{t} depends both on the accuracy of f_{v} and t_{peak} and can vary. Furthermore y_{t} should be rounded to an integer (we can only display an integer number of lines on a PC screen) which introduces further errors. Our definition for y_{t} is

$$y_{\mathrm{t}} = \left\| \frac{1}{t_{\mathrm{peak}} \cdot f_{\mathrm{v}}} \right\| \pm (\delta y_{\mathrm{t}} + 0.5)$$

where 0.5 comes from the rounding. Also the uncertainties in t_{peak} and

f_v are δf since both are being read from the same autocorrelation plot in milliseconds. In order to do error propagation, we need to take the partial derivatives with respect to f_v and t_peak

$$\frac{\partial h}{\partial f_\mathrm{v}} = -\frac{1}{t_\mathrm{peak} \cdot f_\mathrm{v}^2} \quad \text{and} \quad \frac{\partial h}{\partial t_\mathrm{peak}} = -\frac{1}{f_\mathrm{v} \cdot t_\mathrm{peak}^2}.$$

So for the uncertainty in y_t, we have

$$\delta y_\mathrm{t} = \sqrt{\left(\frac{\partial h}{\partial f_\mathrm{v}}\delta f_\mathrm{v}\right)^2 + \left(\frac{\partial h}{\partial t_\mathrm{peak}}\delta t_\mathrm{peak}\right)^2} = \sqrt{\frac{1}{f_\mathrm{v}^2} + \frac{1}{t_\mathrm{peak}^2}} \times \frac{\delta f}{f_\mathrm{v} \cdot t_\mathrm{peak}}.$$

We can also observe that the larger the sample rate gets, the smaller δf and δt get.

Chapter 4

Practical attack

Before explaining how the software works internally, let's present a demonstration of a practical video eavesdropping attack. Its main aim is to show the ease with which such an attack could happen. In the meantime this will give an opportunity to explain the characteristics of the received signal and how they are exploited.

The demonstration is undertaken in controlled conditions. However, in order to make it as similar to a real-world attack as possible, we will assume the adversary has no knowledge of the victim's system. We will estimate the frequency at which the emission strength peaks. We will then analyse the signal to detect the resolution and refresh rate of the screen. We will afterwards lock onto the signal and try to recover the original video.

4.1 The Set-up

The choice for a front-end for this demonstration is a USRP B200[1]. Depending on the particular requirements, an attacker might prefer mobility over accuracy and choose the smaller Mirics FlexiTV^{TM}MSi3101 USB Dongle.

[1]Refer to 5.1 Hardware for discussion on currently available devices.

However, for this demonstration we will attempt to obtain the highest possible resolution. Therefore we need a radio that is capable of obtaining a wide bandwidth. This makes the 32 MHz of bandwidth that the USRP provides a much better choice than the 8 MHz available from the Mirics dongle.

For an antenna, we will choose the portable MaxView active TV antenna. It is designed for digital television reception and has a built-in amplification. This is very useful for lifting signals above the USRP B200 noise floor. For better reception from longer distance, a suitable log-periodic antenna, an amplifier and a band-pass filter could be used for preconditioning. This can make the system less portable. However, the MaxView antenna is a cheaper choice and in the end did the required job.

You can view the equipment used by the adversary, the target and their mutual position on Figure 4.1. We now take the place of the adversary that has set up their system, connected the UHD to the laptop and the antenna to the UHD and has launched the *JTempest.jar* executable.

4.2 The Attack

We should now see the GUI as in Figure 4.2. In order to start the USRP B200, we need to go to *File* and choose *Load USRP (via UHD)*. We can enter the command *–rate=8000000* which will set the sampling rate to 8 MHz. If no errors occur, we will see the "Start" button becoming active. Once we press on the button, the system will start processing the data sampled by the USRP.

If we knew the resolution, frame-rate and the frequency at which the emanations from the target occur, we could enter them directly into the GUI and the story would end here. However, since we don't, we need to estimate them. That's why we started with a low sampling rate (8 MHz). Such mode will not be good for actual eavesdropping since it will not provide the full resolution, however this will allow for improved interactivity and for faster autocorrelation results.

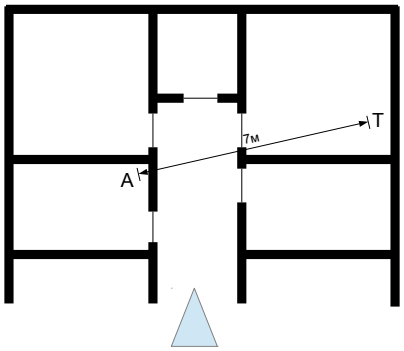

The floor plan

The hallway (triangle)

Target (T)

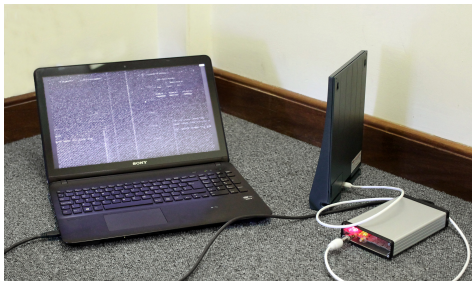

Adversary (A)

Figure 4.1: The figure represents the set-up of the attack. The floor plan shows the position of the attacker and the target. The distance between them is 7 m and the signal passes through two solid walls. The target is a standard PC, connected to a normal VGA monitor. The adversary uses a laptop, a USRP B200 and a MaxView TV antenna. All is inexpensive off-the-shelf equipment. The set-up also allows for great mobility.

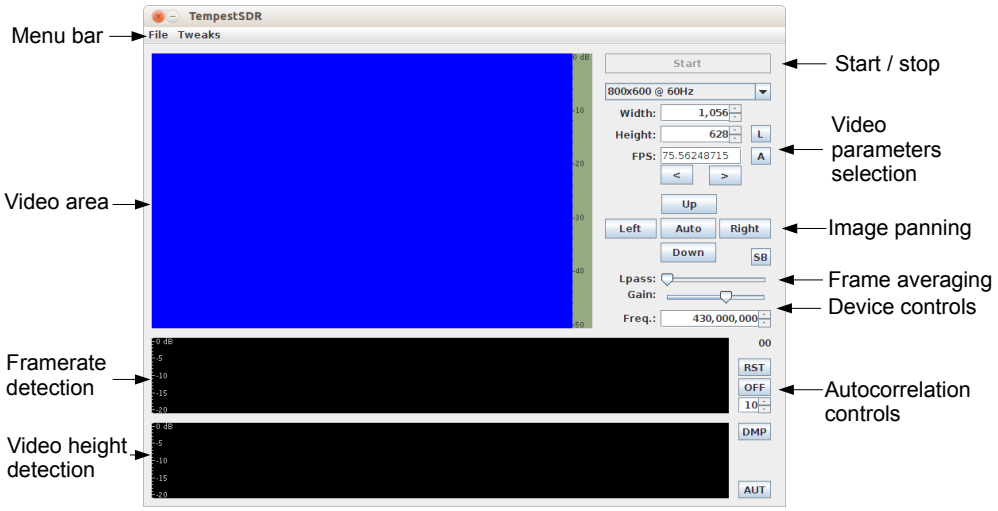

Figure 4.2: The interface of the program. The "A" button will enable the frame-rate tracking feature. The "Auto" button will attempt to detect synchronisation regions. The "AUT" button will try to automatically detect the resolution and line rate (video height). The scale on the right of the video shows in real-time the grey-scale values that map to a particular sample intensity.

First, we need to estimate the frequency at which the emanations from the target peak. To do that we need to keep an eye on the autocorrelation plot and keep changing the frequency until a promising signal appears. There would be a lot of background signals so this would be challenging. However, most video displays run at known refresh rates of 60 Hz, 75 Hz or 71 Hz. If we spot a signal near these values, then we know we are on to something. Figure 4.3 shows that there might be a possible signal onto the current frequency of 125 MHz.

In order to set the video parameters to the frequencies in those spikes, we just need to click with the mouse on top of them. We can inspect the frequency at a certain position by hovering the mouse on top. Once we select the best candidate for the refresh rate, we can now choose the best candidate for the line rate as well. This defines the height of the video frame. Note that we can try the "AUT" button which will simply choose the highest values of the two plots. However, when the signal-to-noise ratio is low, other repeating signals

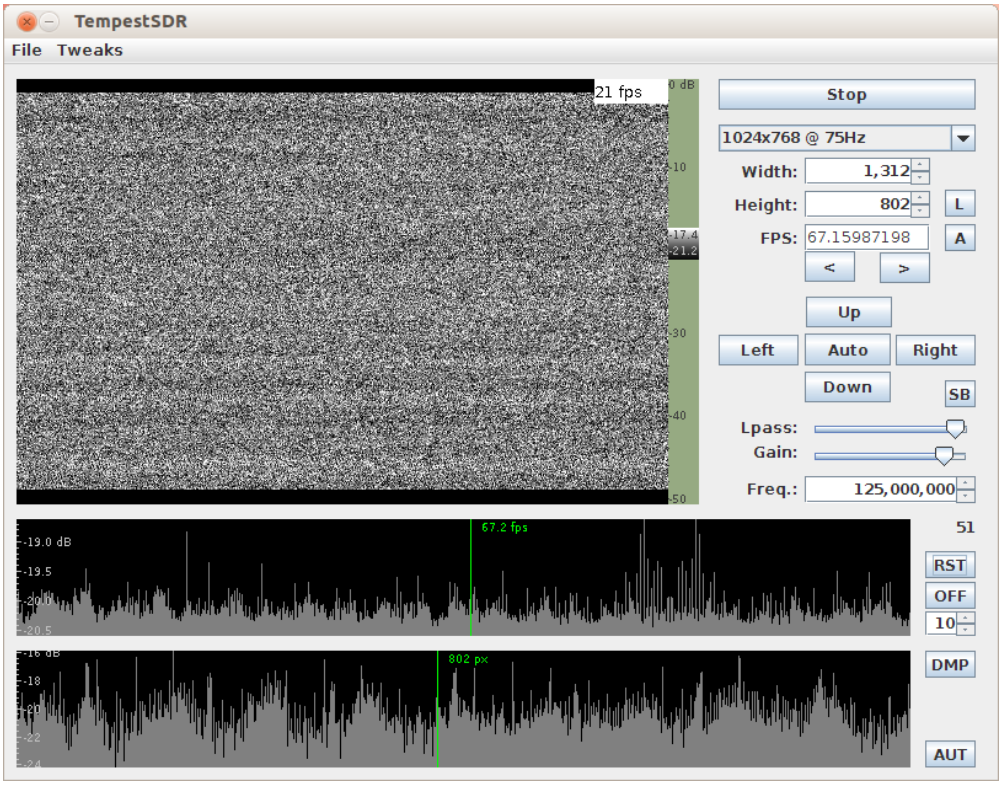

Figure 4.3: We can see two spikes in the top autocorrelation plot around 60 fps that is responsible for the target refresh rate.

on the same frequency may be more prominent so manual adjustment would be required. The autocorrelation plots are interactive and the user can zoom with the mouse wheel and pan around for choosing small details in the plots. Now we click on the 60.3 fps spike on the top plot and the 628 px spike on the bottom one.

If we turn on the "Lpass" averaging, we will get rid of most of the noise and improve the signal-to-noise ratio bringing up the weak video signal (Figure 4.4). We can clearly see the synchronisation pulses. We are also only seeing rapid changes in colours, so we know this is an analogue signal. Digital signals will also show activity in regions that have constant intensities. That's why digital signals could be eavesdropped easier – they emit more energy because of the sharp edges of the individual bits. However, we are apparently dealing with a VGA signal with resolution 800×600 @ 60. Note that the system

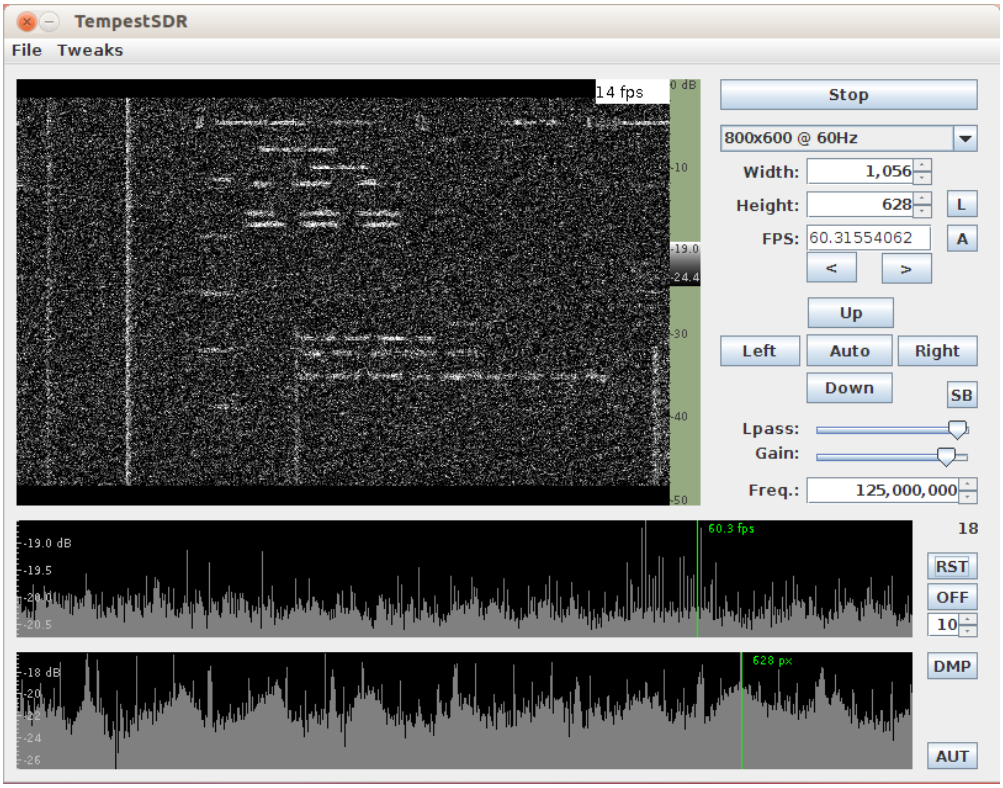

Figure 4.4: We can see two spikes in the top autocorrelation plot around 60 fps that is responsible for the target refresh rate.

auto-detected it (it shows up in the list underneath the "Stop" button).

We see another autocorrelation peak at 61 Hz. This is aliasing due to the two strong synchronisation lines that appear in the video (you can see them on the left). By clicking on the other peak, we can indeed confirm our suspicion that it is just aliasing. Now that we have a signal, we can try to improve it. Since the signal is strongly polarized, changing the antenna angle and position can have a dramatic effect on the end result. Now we can increase the sampling rate of the USRP to improve the resolution of the obtained image.

4.3 Conclusion

If we obtain a good enough signal, we can reconstruct text from the screen. Compare on Figure 4.5 the actual image shown on the target screen and the best estimate obtained from the hallway just outside the room with the target with 32 MHz sampling rate. We can in fact clearly read the text in the text editor.

This shows that a practical attack is possible even from an adversary on a low budget with very little knowledge of the DSP. We also demonstrated that we can deduce the video parameters of a screen remotely in a real-world environment. A more sophisticated attacker, could use better equipment with a lower noise floor and higher antenna gain to undertake such an attack from an even further distance. This should open the discussion about what could be done to prevent compromising emanations leaking from cables.

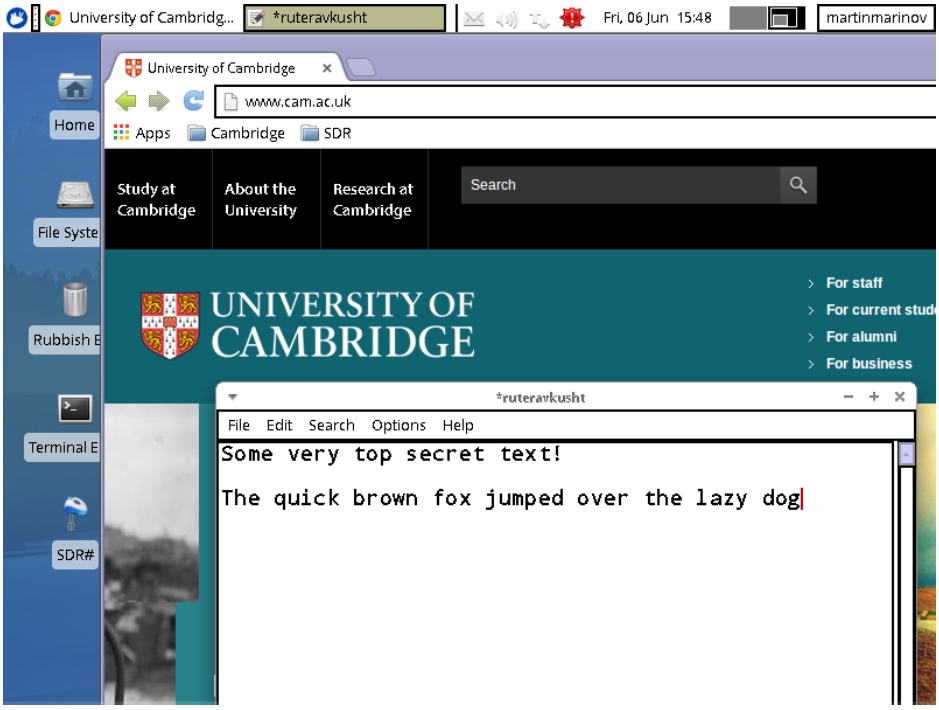

(a) Screen shot of the target monitor.

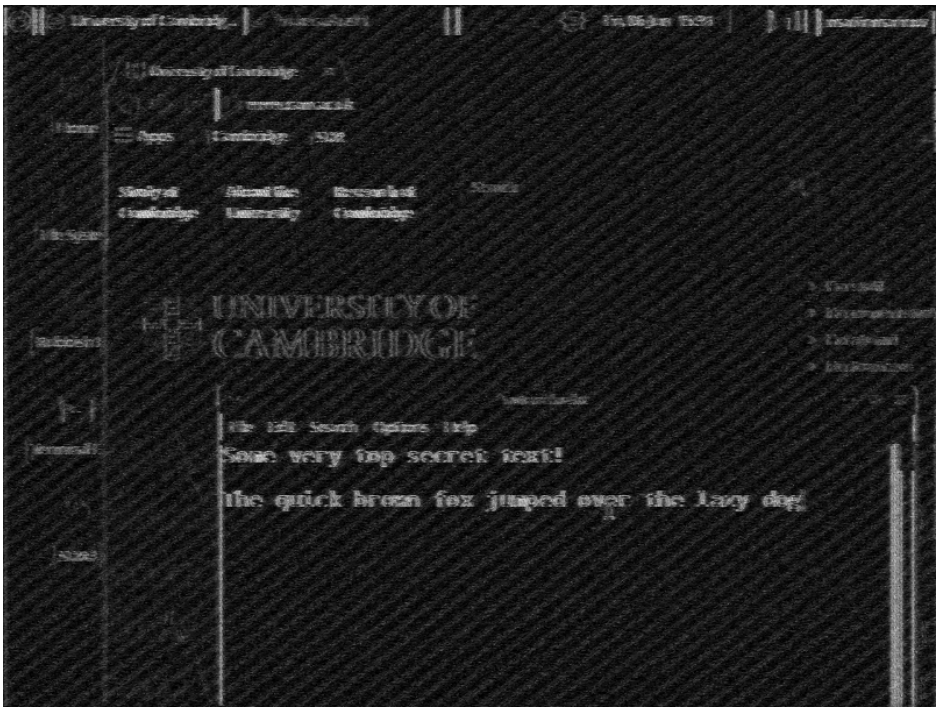

(b) Best result (blanking cropped out).

Figure 4.5

Chapter 5

Implementation

5.1 Hardware

Figure 5.1: From left to right: MSi3101, AverMedia antenna and USRP B200

There is a wide range of off-the-shelf hardware front-ends that could be used with the system. An attacker can choose one depending on their require-

ments. A quick overview of some supported available hardware is outlined below.

5.1.1 Ettus Research USRP

Maximum sampling rate:	56 MHz (for B200)
Frequency Range:	70 MHz - 6 GHz
Dimensions:	97 mm × 155 mm × 15 mm (for B200)
OS support:	All platforms (Windows support via ExtIO)
Dropped samples detection:	Yes (Except on Windows)

The maximum sampling rate varies between the different models as well as the dimensions. I have used the USRP B200 throughout this report.

Pros:

- A variety of models available in multiple price ranges.
- High enough sampling rates for most eavesdropping scenarios.

Cons:

- Some models need external power supply. B200 in particular does not.
- May need some analogue preconditioning for good eavesdropping results.

5.1.2 Mirics FlexiTV^{TM}MSi3101

Maximum sampling rate:	8 MHz
Frequency Range:	64 MHz - 240 MHz and 470 MHz - 960 MHz
Dimensions:	25 mm × 80 mm × 10 mm
OS support:	Windows only
Dropped samples detection:	Yes

It is the best low end solution but it won't achieve the receiving distance or the quality that one would get with a higher end device.

Pros:

- Portable and unsuspicious looking – just a typical USB dongle.
- Inexpensive – under £100.

Cons:

- Low sampling rate and low sensitivity. Good eavesdropping results would be obtained if the target screen resolution is low enough so that κ (refer to (3.15) for definition) is reasonable and the signal is strong enough.
- Tuning gap between 240 MHz and 470 MHz. If the emanations fall within this range, the Mirics dongle will fail to pick them up.

5.1.3 Windows ExtIO

The plug-in supports variety of devices. It is a standard plug-in that is used in a number of software-defined radio solutions. However, it does not take into account for dropped samples. This means that if sample loss did occur, this would be very visible on the screen rendering eavesdropping practically difficult. It also only runs on Windows.

5.1.4 Antennas and Preconditioning

For the experiments in this report, I have either used a small, dual-pole antenna by AverMedia, or an active antenna by MaxView, both designed for digital TV reception. This showed to be enough for eavesdropping from an adjacent room to the one containing the target device. However, for impressive demos that could potentially operate from several tens of meters, some additional analogue preconditioning and professional antennas need to be used.

Kuhn experimented with a tunable band pass filter and a 30 dB antenna amplifier before the B200 to improve the noise level. He comments that the

set-up delivers comparable quality to the highly specialised Dynamic Sciences R1250 receiver that he used in his experiments [7]. He also used a professional log-periodic antenna for improved reception.

5.2 Architecture

The whole system consists of two parts - a library (called **TSDRLibrary**) and a host program. The library is the main deliverable of the project. It is responsible for decoding the emanated signal – from obtaining the data from the hardware to processing it. However it can't run as a stand-alone application. It needs a host program to control it via an API (defined in *TSDRLibrary.h*) and to receive the decoded video frames. The host program could be written in any programming language that can use native libraries.

However, the package also comes with a pre-built Java based host program. The provided implementation allows for full manual control over the library via a graphical user interface (GUI). It is very useful for real-time monitoring and interacting asynchronously with the library while the processing is taking place. In practice it is a single executable that has TSDRLibrary built in. This is what the report has been referring to as "the system" so far – the Java GUI combined with TSDRLibrary. An end user would never notice that there is another layer underneath the GUI. All the examples and screen-shots given here have been obtained via the provided Java based GUI while it is controlling TSDRLibrary.

The whole system was designed and developed from scratch entirely by me. It does not rely on or include any third party libraries [1]. Having no dependencies makes it extremely lightweight, portable and easy to compile.

[1] Some IQ source plug-ins may depend on a driver library for the particular device they serve. However, the file input plug-in has no external dependencies, so the system can in fact decode pre-recorded signals without needing any additional software.

5.2.1 The Library

The library relies on plug-ins (called **TSDRPlugin**) to provide a stream of IQ samples and means to control the hardware in real time. The data sources are shared libraries that are dynamically loaded at runtime by the TSDRLirbary.

The host program's job is extremely simplified. In a nutshell, it sets up the library and runs it. Every time there is a new video frame available, a callback would be invoked via TSDRLibrary so that the host program could process the frame (display it, save it, etc). An expected sequence of API calls to get video data would be:

1. Dynamically load the library (if it is not statically compiled with the host program) using the methods provided by the specific operating system. This will give the host program access to the TSDRLibrary APIs.

2. Allocate an instance of the processing pipeline with *tsdr_init*.

3. Set target display resolution and frame rate with *tsdr_setresolution*. This could be called interactively while the processing is running to dynamically change the parameters at runtime.

4. Load a pre-compiled plug-in by invoking *tsdr_loadplugin* specifying the location of the shared library that represents the plug-in and any parameters that the user wants to pass to the plug-in. This plug-in will talk to the hardware and provide a steam of IQ data to the library for processing.

5. Start the processing by running *tsdr_readasync*. The current thread would be used to start polling the hardware so it will block until processing has finished.

6. The *tsdr_init* and *tsdr_readasync* allow for callback functions to be registered with TSDRLibrary. The callbacks are just C functions that reside in the host program that will be called as soon as a new video

frames, autocorrelation data or other messages are available. Processing data within those callbacks is not thread safe.

7. Call *tsdr_stop* to stop the processing and unblock the thread that originally called *tsdr_readasync*. Soon after calling *tsdr_stop*, the callbacks will stop receiving data.

If the plug-in supports it, *tsdr_setbasefreq* can be used to set the base frequency of the hardware device. A few other API commands allow the host program to do manual position adjustment of the video frame, control the amount of low-pass applied and set the gain of the hardware device (if supported). There are some advanced features that could be turned on using the *tsdr_setparameter* API call which include the automatic frame borders detection, automatic frame rate synchronisation and a few other tweaks to the digital signal processing pipeline. It is up to the host program to use the autocorrelation to determine resolution and frame rate which gives enough room for flexibility.

Each API call can return an error code in case it fails. The host application can also read a verbose version of the error message using the *tsdr_getlasterrortext* API call. This allows for intuitive and simple error handling.

5.2.2 Data Flow

Figure 5.2 outlines the data flow and data processing paths within a typical set-up of the system[2]. It goes through the following steps:

1. RF data is converted into IQ samples in the SDR Device. These samples are sent to the PC for processing.

2. The hardware driver in the OS receives the samples and possibly queues them.

[2]If instead the data is read from a file or network, we can regard the "Software - defined radio hardware" as the hard drive or the network layer.

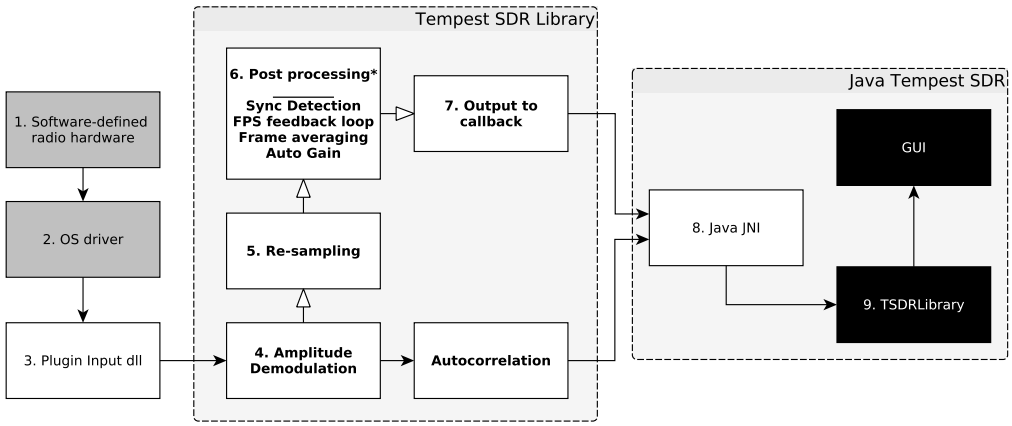

Figure 5.2: Data processing in the system using the Java GUI. Bold text represents different native threads. White background means code is written in C. Black background means code is written in Java. Gray background is for operating system related processes and external hardware. Arrows with white ends represent points where data could be dropped due to performance reasons. Arrows with black ends represent transferring full data that was processed in the previous step. The star on the Post processing stage means that the outlined sub-stages could be executed in different order depending on user preferences.

3. A TSDRPlugin either continuously polls the driver or receives a callback from it as soon as a block of data is available. It obtains the block of data and sends it to the TSDRLibrary via a callback.

4. The IQ data is inside TSDRLibrary. AM demodulation is done on the data. This runs in a separate thread so that the TSDRPlugin will have the chance to receive new data from the device as quickly as possible. The demodulated data is provided to the Autocorrelation thread that will calculate the autocorrelation of the incoming signal and notify the host program. If TSDRPlugin reports any dropped samples between calls, the autocorrelation is reset (we only want continuous data accumulated for autocorrelation).

5. The re-sampling logic runs in a separate thread. It matches the rate of the data from the sampling rate of the device f_s to the expected rate of $x_\mathrm{t} \cdot y_\mathrm{t} \cdot f_\mathrm{v}$.

6. Here some digital signal processing is done in a separate thread to enhance the signal. The order with which the operations are applied depends on the settings that a user will supply. By default the synchronisation pulses of a video frame are detected first. If the user has selected auto tracking, the current position of the horizontal blanking interval is compared with the last one. This gives a rough estimate on whether f_{fps} is off by a couple of parts per million from the real value. The process allows for keeping the picture steady on the screen. Then low-pass in the time domain is done (a.k.a. motion blur) to de-noise a weaker signal using averaging. Finally, an auto gain algorithm makes sure that the full dynamic range of the signal is equally utilised for the final image.

7. Here the host application receives a video frame via a callback. It is up to the host application to determine what to do with it. It can take as much time as it wants since this runs in a separate thread.

8. The signal leaves the library and goes into the host application. In this example this is our Java GUI. A Java Native Interface (JNI) code marshals the incoming data to a Java friendly format which is then passed to the Java Virtual Machine and the particular class instance that has invoked the whole processing.

9. Once the data arrives at the TSDRLibrary class instance, the main GUI will receive a notification via a callback and will dispatch the bitmap to be drawn on the screen.

The biggest problem faced was synchronising dropped samples. To illustrate the issue, imagine we are receiving samples at a rate of 50 mega samples per second. If each sample contains two floating point values (the I and the Q component), each of which being 4 bytes of data, then the total data rate coming from the hardware would be $8 \times 50 = 400$ megabytes per second! This is a huge amount of data. Since the configuration is running on a non-real-time operating system, the CPU might not be able to cope with such a fast stream. Furthermore there could be some hardware limits enforced as

well, for example maximum throughput of the data bus that is being used to transmit the data from the device to the PC.

This means that we will have a lot of dropped samples coming from the device. At the same time, even if we don't have any dropped samples, the CPU can still fail to process all the desired data in real-time. This means that, in order to have the system run interactively, some samples that can't be processed in real-time should be dropped. This would allow for fresh data to be collected for processing. However having even a couple of dropped samples is a problem. This is because video is continuous. Dropping a few pixels means that the whole frame synchronization could be broken.

Therefore the library employs an algorithm that allows it to drop samples only an integer multiple of $x_\mathrm{t} \times h$ at a time. This means that even if a single sample was dropped before processing, the algorithm will enforce a whole batch of $x_\mathrm{t} \times h$ samples to be dropped instead. This means that when the next frame arrives, it will start processing from where the previous frame had dropped samples. Therefore the picture will look seamless to the end user since the dropped samples will actually result in a lower frame-rate in the host application. This approach allows the system to run even on not so powerful configurations and still produce some output. Such synchronization points are denoted as white arrows on Figure 5.2.

5.3 Digital Signal Processing

Re-sampling

Digital re-sampling is used as the processing step that synchronises the incoming sample rate $f_\mathrm{s} = t_\mathrm{s}^{-1}$ to the desired pixel rate $f_\mathrm{p} = t_\mathrm{p}^{-1}$. Let's imagine each incoming sample contains information about a fraction a^{-1} of a pixel. Each output sample will then contain the information from a incoming samples so that it will form a single pixel. Alternatively if b pixels are contained in an incoming sample, the re-sampling will generate output of b samples for

each incoming sample.

The re-sampler sees a stream of samples coming at a rate f_s, interpolating their rate with f_p and then decimating the resulting stream (that now has sampling rate $f_\mathrm{s} \cdot f_\mathrm{p}$) by a factor of f_s. This results in an output stream of rate $f_\mathrm{p} = t_\mathrm{p}^{-1}$. Each sample then will relate to a pixel value at that time. In mathematical terms,

$$v[n] = x\left[f_\mathrm{s} \cdot \frac{n}{f_\mathrm{p}}\right],$$

where ($n \in \mathbb{Z}$) and $v[n]$ are the output pixel intensities [3] and

$$x[n] = \sqrt{I_n \cdot I_n + Q_n \cdot Q_n}$$

are the incoming sample intensities. If this algorithm is implemented straight away, it would be called **nearest neighbour** re-sampling. Unless $x[n]$ is band limited to $\min(f_\mathrm{p}, f_\mathrm{s})$, $v[n]$ will contain aliasing artefacts. Therefore, as a pre-processing step, we can apply a low-pass filter to $x[n]$ with a cut-off frequency $\min(f_\mathrm{p}, f_\mathrm{s})$ as an anti-aliasing filter.

A perfect low-pass filter uses sinc interpolation. However, in practice, it is not achievable since sinc is an infinite function in the time domain. There are some good approximations using windowed sinc functions. However, applying these is expensive since the related algorithms are based on convolution. Luckily, there is a computationally cheap approximation of a low-pass filter that could be done during re-sampling. It uses linear interpolation between two consecutive samples to reduce the aliasing artefacts. The actual implemented re-sampling algorithm in the project utilises the Brasenham's line algorithm[21] to achieve non-integer re-sampling.

There is another trick that is done to improve the anti-aliasing quality and possibly performance. Since the x_t of an image is only used to maintain the aspect ratio, the library assumes that $x_\mathrm{t} = \hat{x}_\mathrm{t} = \lceil \frac{f_\mathrm{s}}{f_\mathrm{v} \cdot y_\mathrm{t}} \rceil$. This allows the host program to use whatever algorithm they desire to re-sample the output image to any resolution. Since the host program can use GUI acceleration for

[3] Note that the notation $v[n]$ is equivalent to the previously used v_n.

the re-sampling process, it can afford more expensive algorithms that result in less aliasing artefacts. Furthermore, when $f_\mathrm{p} > f_\mathrm{s}$ as in most real-world eavesdropping scenarios, the CPU will have to handle less data resulting in improved performance.

Auto Gain

The auto gain step ensures that the image uses the full dynamic output range. For example, if demodulated pixels $v[n]$ have the property $v_\mathrm{min} \leq v[n] \leq v_\mathrm{max}$ then we can construct a new stream of pixels $v'[n]$ such that

$$v'[n] = \frac{v[n] - v_\mathrm{min}}{v_\mathrm{max} - v_\mathrm{min}}$$

which now means that $0 \leq v'[n] \leq 1$. This is then handed over to the host program which can show interactively the relationship between $v'[n]$ and $v[n]$. This is used by the Java GUI to show the relationship between the displayed gray-scale values and the incoming samples strength.

Frame Averaging

The time averaging applies an infinite impulse response (IIR) low-pass filter to a stream of input pixels $v[n]$ to produce a stream of output pixels $v'[n]$ such that

$$v'[n] = \alpha \cdot v[n] + (1 - \alpha) \cdot v'[n].$$

This does inter-frame averaging sometimes known as motion blur. It attenuates random noise between consecutive frames and amplifies the constant signal, thus increasing the signal-to-noise ratio. The weight of the filter could be adjusted by changing α from 0 to 1.

5.3.1 Synchronization Detection

In order to detect the blanking intervals in a frame, a few assumptions need to be done. What is characteristic about the intervals is that they do not contain any activity compared to the video region. This means that usually they are seen as a band of solid colour (see Figure 5.3). They either contain more energy than the video region or contain less energy. Therefore we can assume that the average intensity of the blanking interval is very different from the intensity energy in the video region.

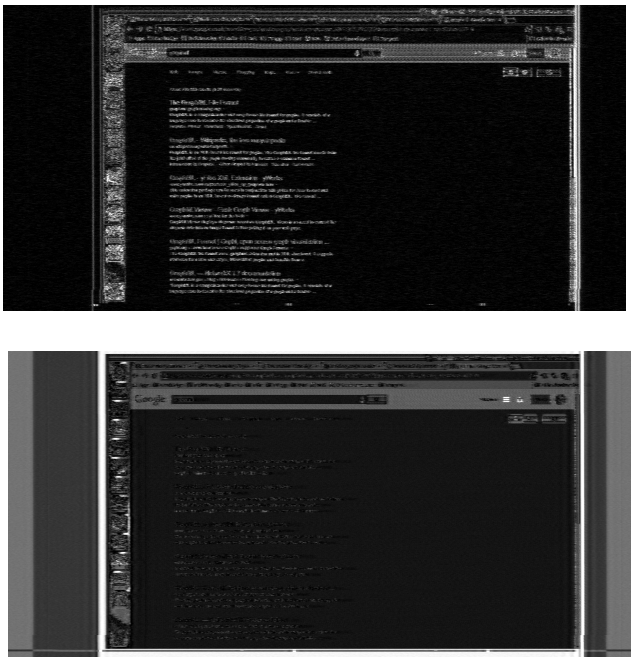

Figure 5.3: Compare the blanking interval of the same digital signal, centred at two different frequencies of the spectrum. One of them looks dark, while the other one is lighter and has some bands. The similarity is that they are very smooth and do not contain high frequency intensity changes.

In order to detect the intervals, for performance reasons, we can decouple them into two 1 dimensional strips. We produce two strips – a vertical one, containing the average of all the lines and a horizontal one, containing the average of all the columns in an image. Then we can do a circular low-pass filter in order to get rid of any high frequency noise (such as text lines).

Figure 5.3 shows how the averaged vertical and horizontal bands are derived and how they look after the low-pass filter.

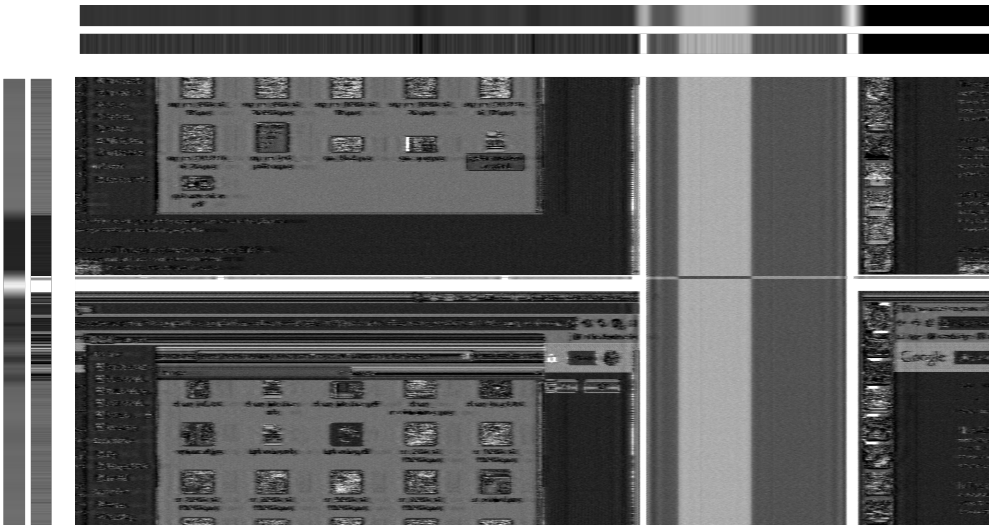

Figure 5.4: In order to detect blanking regions, first an average of the vertical and the horizontal pixels is taken. Then this average is blurred using a low-pass filter with a Gaussian kernel.

Now we can use the assumed property that the blanking regions have the most different average intensity compared to video regions. Let's say a band has n elements $b[n]$. We now need to partition the two bands into two regions with width $2w$ and $n - 2w$, centred at c and $n - c$. Then the value of the average per pixel difference would be

$$\beta(w, c) = \left[\sum_{k=c-w}^{c+w} \frac{b[k \mod n]}{2w} - \sum_{k=2w-c}^{2(n-w)-c} \frac{b[k \mod n]}{2n - 4w} \right]^2 .$$

We need to choose $2w$ and c so to maximise β. Since the constraint is $0 \leq 2w < n$ and $0 \leq c < n$, we can in fact calculate β for each possible input and find the parameters that maximise it. This is an algorithm complexity of $O(n^2)$ which explains why we decided to do that on two 1D arrays rather than on the whole 2D image.

However that algorithm won't always do the job. Imagine the video signal has a strong component with a very short size. This can easily be a value that

maximises β. But we know that synchronisation regions are not that small, therefore we need some lower bound constraints for the size of a blanking region. By observing various video signals, I came up with some arbitrary numbers of $5\% \times x_{\mathrm{t}}$ for horizontal blanking and $1\% \times y_{\mathrm{t}}$ for vertical blanking. These number can be adjusted (in the source code) depending on the judgement of the eavesdropper, but so far they have shown to perform well.

We can't easily change the asymptotical growth of the algorithm. However, we can reduce its execution time by putting some additional constraints. Let's assume that the blanking region is always smaller than the video region and we use $2w$ to denote the width of the blanking region. This will put an upper bound for the value of $2w < \frac{n}{2}$. Having a lower and upper bound for $2w$ means that now the algorithm can run faster, in real time, for both strips. Figure 5.5 shows how the value of c, the position of the synchronisation region in a frame, looks like in practice for a given set of data. This value is used to center the frame in the GUI video window in the vertical and horizontal position (Figure 5.6).

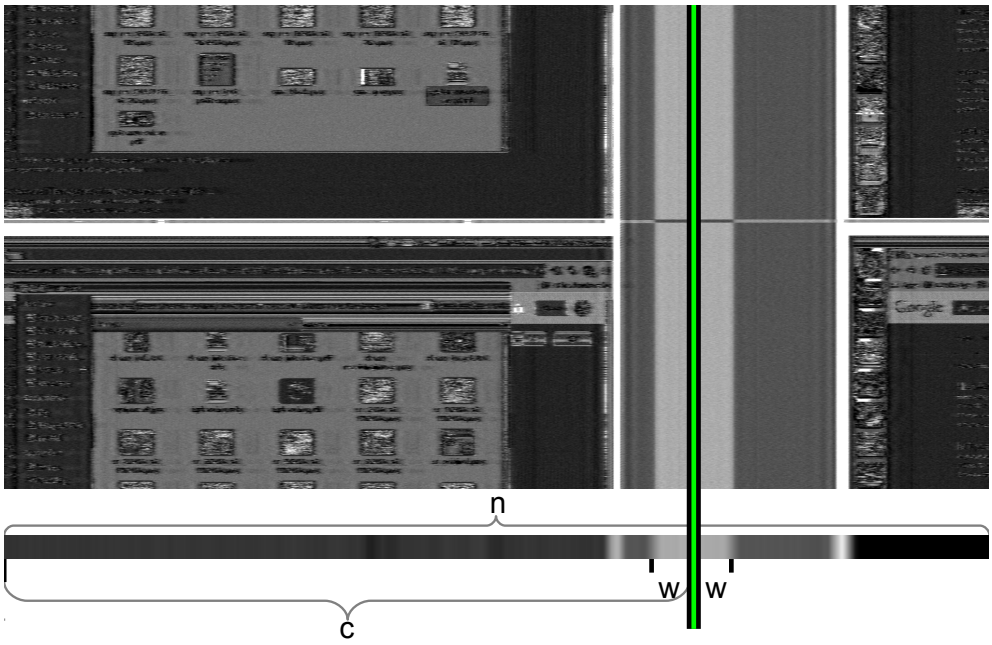

Figure 5.5: Visualising the relationship between c, w and n. The figure shows the values for w and c that give the maximum value of β for the frame.

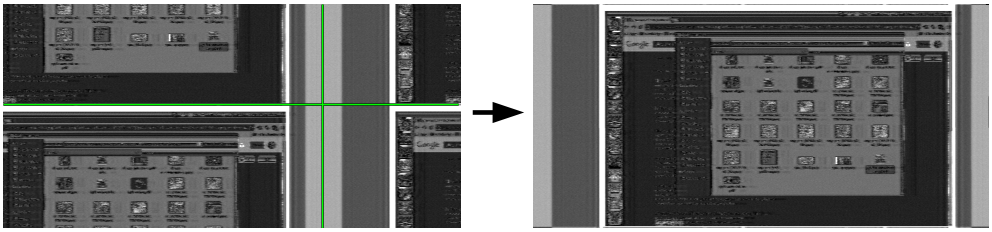

Figure 5.6: Given the value for c for the vertical and the horizontal strips, we can dynamically align the frame in the real-time video display.

5.3.2 Tracking the Frame Rate

The drift between the local oscillator and the pixel clock of the target will cause the image to accelerate slowly over time. This could be automatically compensated. It only works once we have a stable video image and we can reliably estimate c. If we say that the value of c for frame number n is $c[n]$, then we can take the speed with which the synchronisation frame is moving across the screen which is simply

$$\frac{\mathrm{d}c[n]}{\mathrm{d}n} = v_{\mathrm{c}}[n] = c[n] - c[n-1].$$

If $v_{\mathrm{c}}[n] > 0$ then we know that our estimate $\hat{f}_{\mathrm{v}}$ for f_{v} is $\hat{f}_{\mathrm{v}} > f_{\mathrm{v}}$ and if $v_{\mathrm{c}}[n] > 0$, then $\hat{f}_{\mathrm{v}} < f_{\mathrm{v}}$. Since we don't know the true value f_{v}, we can try to approximate it by adjusting our estimate $\hat{f}_{\mathrm{v}}$ with a function $a[v_{\mathrm{c}}]$. Therefore at each frame we can change our estimate to be

$$\hat{f}_{\mathrm{v}} = \hat{f}_{\mathrm{v}} - \mathrm{sgn}(v_{\mathrm{c}}) \cdot a[v_{\mathrm{c}}]$$

where $\mathrm{sgn}(x)$ is the sign function, that returns $+1$ if $x \geq 0$ and -1 if $x < 0$. We should note that $a[v_{\mathrm{c}}]$ will depend on the particular heuristics used. My implementation uses two-speed modes, having a low speed for slow moving drift for accuracy and a high speed for fast moving frames. The output of my implementation of $a[v_{\mathrm{c}}]$ is also proportional to the magnitude of the speed itself.

This generates a self-correcting feedback loop. Any perturbation will cause

the system to adjust itself and lock. However, $a[v_c]$ needs to be chosen carefully to avoid oscillations. The latency of the processing also increases the chances of obtaining oscillations since the change in $\hat{f}_v$ will not be propagated immediately to the next frame. The exact values I have used do cause oscillations in some scenarios so it would be a nice research attempt to find a good value for them. This was a minor issue that was left outside the scope of the project.

5.3.3 Autocorrelation

We can remind ourselves that the autocorrelation was defined in (3.16). However, in practice we only have a finite number of samples n, so we can rewrite the formula so that it reads

$$R_{vv}(\tau) = \sum_{i=0}^{n-1} v_i \bar{v}_{i-\tau}.$$

We need to recalculate $R_{vv}(\tau)$ for every value of τ from 0 to $n-1$ and this will give us our autocorrelation plot. If we naively implement this, we would see that the performance of the algorithm is $O(n^2)$. This means that the real-time performance will be problematic.

The Wiener-Khintchine theorem [22] allows for another definition of $R_{vv}(\tau)$ using Fourier transforms

$$\begin{aligned} V_k &= \mathcal{F}\{v_i\} \\ S_k &= V_k \bar{V}_k \\ R_{vv}(\tau) &= \mathcal{F}^{-1}\{S_k\} \end{aligned} \tag{5.1}$$

where $\bar{V}_k$ is the complex conjugate of V_k and $\mathcal{F}\{v_i\}$ is the discrete Fourier transform that is equal to

$$V_k = \mathcal{F}\{v_i\}(k) = \sum_{i=0}^{n-1} v_i \cdot e^{-j2\pi k \frac{i}{n}}$$

and $\mathcal{F}^{-1}\{S_k\}$ is the inverse discrete Fourier transform defined as

$$R_{vv}(\tau) = \mathcal{F}^{-1}\{S_k\}(\tau) = \frac{1}{n}\sum_{k=0}^{n-1} S_k \cdot e^{j2\pi\tau\frac{k}{n}}.$$

Since the discrete Fourier transform could be computed in $O(n\log(n))$ using an algorithm called Fast Fourier Transform, then we have a way of computing the autocorrelation with complexity $O(n\log(n))$.

When we compute the autocorrelation, we will have a lot of data to visualise. It is safe to assume that refresh rates and line rates of modern displays fall within a bounded range of frequencies. We can use that to limit the amount of data shown interactively on the screen. This not only improves performance, but also simplifies the user's task of understanding the autocorrelation plot since now, rather than showing the plot in terms of milliseconds or frequency, we can display it in "frames per second" and "pixels". Refer to Figure 5.7 to how the actual value of $R_{vv}(\tau)$ is displayed in a user friendly way onto the GUI.

In order to display the data user-friendly, we need to make some assumptions about the possible values of f_v and y_t. The assumption is that videos displays frame rates are constraint to being between f_min fps and f_min fps, therefore we can safely choose $f_\mathrm{min} \leq f_\mathrm{v} \leq f_\mathrm{max}$. There also constraints about the maximum and minimum height of the image y_t, so we can choose $y_\mathrm{min} \leq y_\mathrm{t} \leq y_\mathrm{max}$.

The autocorrelation τ has units of milliseconds and τ^{-1} has units of Hz. This will match the units of f_v exactly, so for displaying the information about the refresh rate, we can use values of τ for which $f_\mathrm{max}^{-1} \leq \tau \leq f_\mathrm{min}^{-1}$ (the green region in Figure 5.7). For a line rate of y_t, the corresponding τ value would be

$$\tau = \frac{1}{y_\mathrm{t} \cdot f_v}.$$

However, since we don't know what the value of f_v is, we can safely say that for displaying the line rate on the GUI we can use values of τ for which

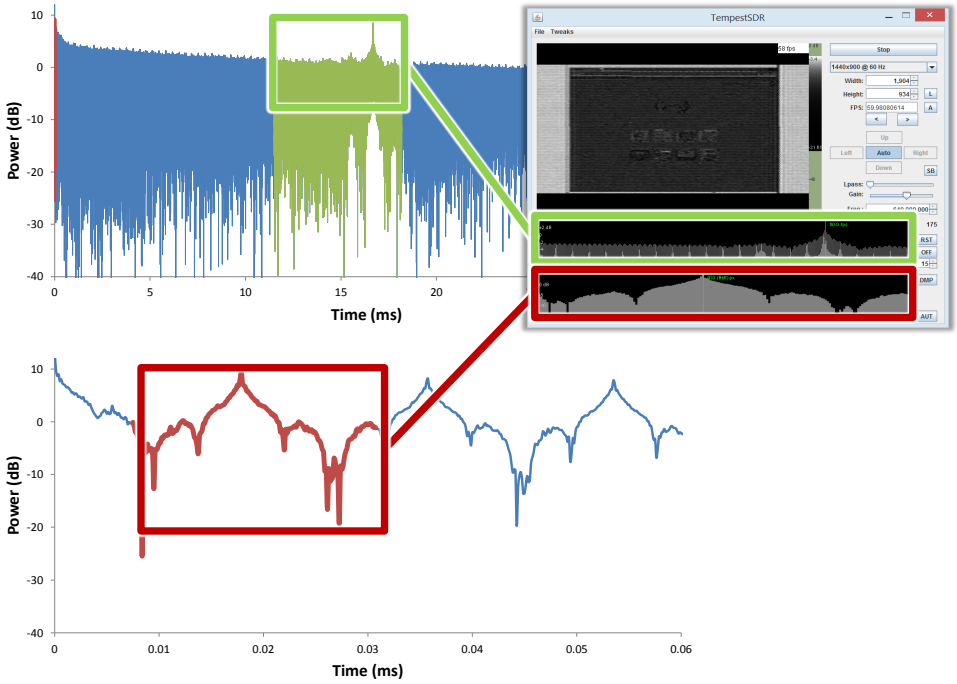

Figure 5.7: We can see how the autocorrelation is plotted on the screen. The green part is used to determine the frame rate f_v and is displayed to the user in units of frames per second. The red part is a zoomed-in version around $\tau = 0$ and it describes the repeating nature of the lines so it can be used for showing the line rate y_t or the height of the image in units of pixels.

$(f_\mathrm{max} y_\mathrm{max})^{-1} \leq \tau \leq (f_\mathrm{min} y_\mathrm{min})^{-1}$ (the red region in Figure 5.7).

Now when the user clicks on a point in the plot, the system calculates the value of the frame rate or the line rate and uses that to update the video parameters interactively. The user can also "zoom" into the plots with the mouse wheel. Moving the mouse over the plot will show the value of $R_{vv}(\tau)$ at that position in dB and τ expressed either as frames per second or pixels depending on the plot that the user is currently interacting with.

The value of x_t, as discussed before, cannot be easily deduced from the autocorrelation plot. However, given y_t and f_v, we can find the closest mode that matches those values in a list of potential video modes (such as the one provided by VESA [17]). The x_t value for that particular mode can be used

to provide the aspect ratio of a video frame. The estimation of the three parameters y_t, f_v and x_t allows for the fully automatic video mode detection implemented in the project.

5.3.4 Multithreading

The multi-threading itself relies on a multi-platform library that I have written to work on Linux, Windows and OS X. It provides abstractions about thread synchronisation primitives and allows starting and controlling threads on all the platforms. However, the most interesting aspect is the way the threads share the data they are processing. This is handled by a thread safe circular buffer which has been unit tested. Each pair of interconnected threads share a different instance of the circular buffer structure.

A thread requests some input data for processing by asking the circular buffer structure that connects it with the previous thread. The call will block until data is available or a time-out has occurred. This ensures that threads are not constantly polling, rather they are using OS level thread synchronisation techniques to sleep when they are processing data faster than real time.

When the thread finishes processing the data it received, it needs to pass the output to the next thread. This is done via the circular buffer that connects the current thread with the next one. The difference here is that this call may fail if the circular buffer is full. This indicates that the output data was actually dropped. The circular buffer can be used to drop additional samples so a full frame containing $x_t \times y_t$ will end up being dropped. This allows taking into account dropped samples that occur in the hardware level as well as dropped samples due to CPU not being able to handle the data in real-time.

There are a few other performance tweaks. The circular buffer can grow if it sees that such drops occur. There is a limit that the buffer can grow to in order to ensure that only near real-time data is being processed. The size of the circular buffer correlates to the latency in the system – the longer

the buffer is, the more latency the system will see. However if the system is fast enough, this mechanism ensures as little latency as possible (and as little memory being used). If the system is slower and can't handle real-time, the latency is increased to allow for additional stages to have more time to process the data. This will result in dropped frames but ensure an interactive system. This is basically a method to relieve the "back pressure" on the system.

5.4 Experimental Results

For performance benchmark, the system was tested on an Intel Core i5 laptop running in real-time, with more than 40 fps with a sampling rate of 25 MHz and RAM usage of less than 256 MB (including the Java runtime). A frame-rate of more than 20 fps can be achieved on a standard desktop Intel Core 2 CPU. This ensures it the performance on any modern hardware provides sufficient interactivity.

During my experiments with real life devices, I made some interesting observations I think are worth sharing. The results are not representative since they are related to the particular equipment I used, but since no screen-shots of some signals are available in the open literature, they can serve as a reference for further research.

VGA signals can be eavesdropped as we saw in Figure 4.5. However, the smooth nature of the analogue signal does not radiate enough power in low contrast regions, leaving only rapid colour transitions visible. This means that the signal carries less energy and is more difficult to detect and eavesdrop. We can see the contrast changing in the horizontal direction but no change could be observed in the vertical. This is due to the fact that pixels are transmitted from left to right.

Digital signals are a bigger thread since individual bits contain sharper edges. Even solid colours will show up because they contain a bit pattern. This could be seen in Figure 3.1 and Figure 5.9 where the signal is very likely the HDMI

cable of the HDMI to VGA converter that is being eavesdropped. Here the relationship between transmitted pixel colour and observed pixel intensity is highly non-linear. However, there are some colours that maximise the contrast.

While experimenting, it turned out the LCD monitor I was using emitted its own signal in addition to the VGA it was receiving. It is very likely an LVDS signal. This could be seen in Figure 5.8. The phenomenon was described by Markus Kuhn [9]. He noted that the vertical blanking interval may not be an integer multiple of the line rate, causing a horizontal "jump" after each frame. The emissions, however are only receivable at very close distances to the monitor (within about a meter). Kuhn has also shown that LVDS emissions from some laptops could be much stronger and are receivable up to tens of meters away [7].

Font aliasing plays an important role in the sharpness of the eavesdropped signal. Kuhn has discussed the issue in detail and even proposed font smoothing as a way to protect from eavesdropping attacks [7]. In Figure 5.9 we can see a comparison of the HDMI signal from 3.1 with font anti-aliasing turned on and off. We can see that it is considerably more difficult to read the text if the font is anti-aliased.

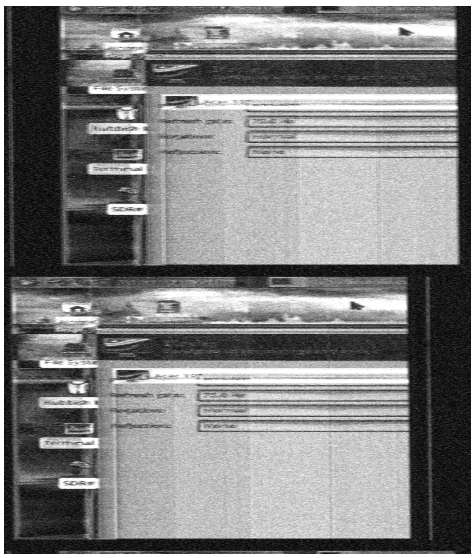

Figure 5.8: LVDS emanation from a monitor. Vertical blanking not constraint to be an integer multiple of the line rate [9]. We need to capture two frames at a time to get a stable picture.

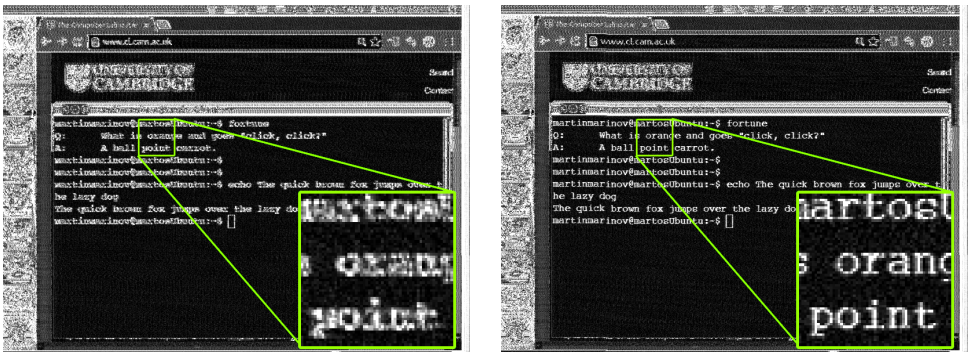

(a) Font anti-aliasing enabled. (b) Font anti-aliasing disabled.

Figure 5.9

Chapter 6

Summary and Conclusions

6.1 Further Research

An idea that proved promising was to try to "extend" the available bandwidth of the software-defined radio front-end. My best attempts in Figure 6.1 show that there is slight improvement. We can take n Fourier transforms of the signal, containing at least one frame in several consecutive bands of width f_s and "merge" the recordings together, creating a new signal that has a bandwidth of $n \cdot f_s$. The requirement is, however that the signals need to be taken at the exact same time. This is impossible with a single receiver of bandwidth f_s. If we, however, assume that the n recordings we have contain the same exact frames, we can align them using cross correlation. However, my experiments show that the aligning is very difficult. Since this was out of the scope of the project, I did abandon the idea. Further research in the area can mean that eavesdropping could be done even with ultra-cheap SDR devices like the RTL2832U based TV dongles that usually only provide up to 3 MHz of bandwidth. This is highly insufficient for real-time eavesdropping.

There were no attempts to compare the quality of the obtained results with existing implementations such as the FPGA based implementation of Markus Kuhn. The reason was the existence of range of different hardware front-ends

(a) Transmitted test image.

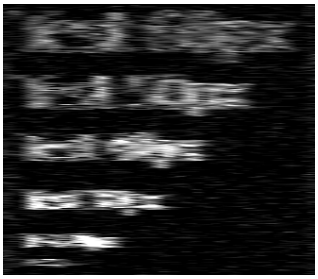

(b) 5 MHz sampling rate.

(c) 5 MHz sampling rate with extended resolution enabled.

Figure 6.1

available for software-defined radio. It is difficult to get hold of some more expensive models that provide a better noise figure and higher signal-to-noise ratio than the USRP B200. The obtained results could be entirely different with one of these receivers. Some research into how to use the system to characterise emanations and possibly measure the exact strengths would be very useful.

Additionally, research into the GUI design suitable for such a system, could be undertaken. This can potentially improve the user friendliness and make the interface more intuitive. There could be, for example, two modes – an advanced mode for professionals, and a simplified mode for end users. A use case for the simplified mode would be users that want to estimate the amount of information their own devices leak into the air.

However, the main aim of the project is to raise the awareness of the issue and demonstrate that it is practically possible. It also serves as a tool for quick prototyping and significantly lowers the costs and efforts related to further research in the area. This would hopefully allow more efforts to be put in discovering methods for reducing the amount of useful information that is emanated from video screens. A nice research topic would be to extend the font smoothing methods that Markus Kuhn proposes [7] as a measure against eavesdropping.

6.2 Conclusion

It is surprising that very little research has been done on the topic of compromising emanations from video displays. This is a real thread that has been around ever since video monitors were first used. Almost every video system has been continuously broadcasting data over the air in clear text. A sophisticated attacker could have already used the vulnerability to steal information without being detected, circumventing traditional cryptographic and physical security. Such an attack could have serious consequences: imagine an adversary eavesdropping a monitor of a bank employee or a voter that is using an electronic voting machine.

The current project has demonstrated that a practical attack is viable from a considerable distance, without the adversary having any prior knowledge about the target. The discussion on how to limit the amount of data leaked started quite late and is currently in its infancy. No official commercially available products exist to safeguard the privacy of users. Military research on the topic remains classified. It is clear that video eavesdropping threads, and threads, related to compromising emanations in general, require more research attention.

The presented project allows research to be done without access to a specialised laboratory. Experiments now only require an affordable, off-the-shelf equipment. The software is open source, allowing anyone to tailor it to their needs. It could be therefore safely concluded, that the project has successfully reached its goal to provide a starting point, much needed for further research on the topic.

Bibliography

[1] CENELEC. Information technology equipment - radio disturbance characteristics - limits and methods of measurement.

[2] Wim Van Eck. Electromagnetic radiation from video display units: an eavesdropping risk? *Computers & Security*, 4(4):269–286, 1985.

[3] Karen Jelved, Andrew D Jackson, and Ole Knudsen. Selected scientific works of hans christian ørsted, 1998.

[4] RFH Nalder. History of the royal corps of signals. *Royal Signals Institution, London*, 1958.

[5] Ross Anderson. *Security engineering*. John Wiley & Sons, 2008.

[6] US National Security Agency. Tempest: A signal problem. 1972.

[7] Markus G Kuhn. Compromising emanations: eavesdropping risks of computer displays. *University of Cambridge Computer Laboratory, Technical Report, UCAM-CL-TR-577*, 2003.

[8] Markus G Kuhn. Electromagnetic eavesdropping risks of flat-panel displays. In *Privacy Enhancing Technologies*, pages 88–107. Springer, 2005.

[9] Markus G Kuhn. Compromising emanations of lcd tv sets. In *Electromagnetic Compatibility (EMC), 2011 IEEE International Symposium on*, pages 931–936. IEEE, 2011.

[10] Fürkan Elibol, Uğur Sarac, and Işın Erer. Realistic eavesdropping attacks on computer displays with low-cost and mobile receiver system. In *Signal Processing Conference (EUSIPCO), 2012 Proceedings of the 20th European*, pages 1767–1771. IEEE, 2012.

[11] National Instruments. Ni pxie-5665 - high-performance vector signal analyzer up to 14 ghz. `http://sine.ni.com/nips/cds/view/p/lang/en/nid/209379`.

[12] Kamaruddin Abdul Ghani, Kaharudin Dimyati, Khadijah Ismail, and Latifah Sarah Supian. Radiated emission from handheld devices with touch-screen lcds. In *Intelligence and Security Informatics Conference (EISIC), 2013 European*, pages 219–219. IEEE, 2013.

[13] Ettus Research. Usrp b200. `https://www.ettus.com/product/details/UB200-KIT`.

[14] James Clerk Maxwell. *A treatise on electricity and magnetism*, volume 1. Clarendon press, 1881.

[15] William L Briggs et al. *The DFT: An Owners' Manual for the Discrete Fourier Transform*. Siam, 1995.

[16] Johan Kirkhorn. Introduction to iq-demodulation of rf-data. *EchoMAT User Manual (FA292640)*, 15:4–10, 1999.

[17] Monitor Timing Specifications. Version 1.0. *Revision 0.8, Video Electronics Standards Association (VESA), San Jose, California*, 1998.

[18] Claude Elwood Shannon. Communication in the presence of noise. *Proceedings of the IRE*, 37(1):10–21, 1949.

[19] G Arfken. Convolution theorem. *Mathematical Methods for Physicists*, pages 810–814.

[20] Ronald Bracewell. The autocorrelation function. *The Fourier transform and its applications*, pages 40–45, 1965.

[21] Jack E Bresenham. Algorithm for computer control of a digital plotter. *IBM Systems journal*, 4(1):25–30, 1965.

[22] Norbert Wiener. *Time Series*. M.I.T. Press, 1964.